1971

Numerical analysis of normal mode helical dipole antennas

Wayne Dennis Swift
Iowa State University

72-12,600

SWIFT, Wayne Dennis, 1944-
NUMERICAL ANALYSIS OF NORMAL MODE HELICAL
DIPOLE ANTENNAS.

Iowa State University, Ph.D., 1971
Engineering, electrical

University Microfilms, A XEROX Company, Ann Arbor, Michigan

Numerical analysis of normal mode helical dipole antennas

by

Wayne Dennis Swift

A Dissertation Submitted to the

Graduate Faculty in Partial Fulfillment of

The Requirements for the Degree of

DOCTOR OF PHILOSOPHY

Major Subject: Electrical Engineering

Approved:

Signature was redacted for privacy.

In Charge of Major Work

Signature was redacted for privacy.

For the Major Department

Signature was redacted for privacy.

For the Graduate College

Iowa State University
Ames, Iowa

1971

PLEASE NOTE:

Some pages have indistinct print. Filmed as received.

UNIVERSITY MICROFILMS.

TABLE OF CONTENTS

I. INTRODUCTION

The characteristics of wave propagation along helical structures have been utilized in several applications, including antennas and traveling wave tubes. In these applications an understanding of device characteristics can be obtained by solving Maxwell's equations subject to the appropriate boundary conditions. The device to be considered here is the normal mode helical dipole antenna (NMHD).

The helical antenna has many possible modes of radiation as discussed by Kraus [1]. The axial mode occurs when the circumference of the helix is on the order of one wavelength and is characterized by radiation along the axis of the helix. In this mode the helix is a broadband antenna, with axial radiation possible over a range of nearly one octave in frequency. An array of axial mode helices was built by Kraus [2] in 1952 for radio astronomy at Ohio State University.

Another possible mode of radiation from a helix is called the normal mode, so named because the maximum radiation is in a plane normal to the axis of the helix. The normal mode occurs when the diameter of the helix is small compared to one wavelength. A NMHD is a helix radiating in the normal mode which is driven at its midpoint.

The NMHD has several characteristics of interest from an engineering viewpoint. Since the helix is a slow wave structure as noted by Collin and Zucker [3], the resonant length of a NMHD is shorter than that for a linear dipole for a given resonant frequency. Thus the NMHD has potential application in size reduction of antennas. Stephenson [4] has characterized this size reduction by shortening factor s. For a NMHD with halflength h in its first resonance, $s = 4h/\lambda_o$ where λ_o is the free space wavelength at the resonant frequency.

The polarization of the radiation from a NMHD is, in general, elliptical, with a large axial ratio when the helix diameter is very small compared to a wavelength. Wheeler [5] has established a design criterion for which the radiation from a NMHD will be circularly polarized.

The possibility of using a NMHD as a superdirective antenna was noted by Stephenson and Mayes [6], who calculated that in its second resonance the NMHD with $s \approx 0.3$ displayed greater directivity than the half-wave linear dipole antenna and that no sidelobes were present. These calculations were based upon an assumed sinusoidal current distribution. Lain, Ziolkowski, and Mayes [7] calculated and measured characteristics of the NMHD in its second and higher order resonances. Their calculations were also based upon an assumed sinusoidal current distribution.

The problem of determining the current distribution along a helix has been approached in several ways. The helix has been approximated by an infinitely long sheath helix, for which Maxwell's equations can be solved, as by Li [8]. Sensiper [9] has an excellent review of wave propagation on helices and includes a solution of the infinite tape helix problem, assuming a real axial propagation constant. Klock [10] also solves the infinite tape helix problem, but for a complex axial propagation constant. Lain, Ziolkowski, and Mayes [7] found that the tape helix solution yielded a better approximation to the resonant frequency of a NMHD than did Li's sheath helix solution. It should be noted that these solutions are for structures of infinite length and are not for a wire helix of finite length.

Marsh [11] measured the current distribution along a helical antenna and interpreted the distribution in terms of three different traveling wave modes along the helix. His T_o mode is that mode which exists on a small diameter helix and displays a large VSWR. Lain, Ziolkowski, and Mayes [7] measured current distribution along several helices and observed an approximately sinusoidal standing wave pattern along the antennas.

At the present time no one has been able to solve analytically the finite length helix with circular conductor as a boundary value problem. As a result, all calculations predicting the behavior of the NMHD are based upon some assumed current distribution, usually sinusoidal. It is the purpose of this work to determine the current distribution for the NMHD by numerically solving the boundary value problem. Other characteristics of interest can easily be calculated from the current distribution.

The antenna considered here is a NMHD where the helix is right-handed, and the conductor is assumed to be copper wire. The NMHD is assumed to be excited at its midpoint by a slice voltage generator as discussed by King [12]. This NMHD is examined in its first two resonant modes and the current distribution, input impedance, bandwidth, efficiency, and directive gain are calculated.

The numerical technique used is the matrix method developed by Harrington [13, 14]. In this method Maxwell's equations are applied to a thin conducting wire. A thin wire is one for which the length is much greater than the radius and the radius is much less than one wavelength.

The wire is then approximated by many segments. Then integrals are approximated by summations and derivatives by finite differences. A linear system of equations is then formed which can be solved to give the current distribution on the antenna for the assumed excitation. Once the current distribution is determined, the field pattern for the antenna can easily be calculated.

Harrington and Mautz [15] used this method to calculate the current distribution for several linear antennas. Strait and Hirasawa [16] applied this method to arrays of linear antennas. The matrix method was applied to arbitrary configurations of bent wires by Chao and Strait [17]. While in principle Chao and Strait's program could be used to solve the NMHD problem, practical considerations dictated that a new program be written.

When many segments are necessary to approximate the antenna, most of the computer time used in the matrix method is consumed in the solution of the linear system to determine current distribution. Since the time required to solve a linear system by elimination is proportional to the cube of the order of the system for large systems, the system should be kept as small as possible if use of excessive computer time is to be avoided. When an antenna is symmetric about its midpoint, the order of the system can be reduced by a factor of almost one-half. Accounting for antenna symmetry thus allows the linear system to be solved about eight times faster than can be done without accounting for symmetry. Also note that the storage necessary for the linear system with symmetry considered is about one-fourth that required if symmetry is ignored. Since the program of Chao and Strait [17] was written for a general antenna, it does not account for symmetry.

In solving a system of linear equations there are three factors which must be considered, especially if the system to be solved is large. These factors are speed, storage required, and accuracy. For a large system the time required to solve the system is approximately equal to $N^3T/3$ for Gauss elimination and equal to N^3T for inversion, where N is the order of the system and T is the machine time required for one multiplication (one complex multiplication if the system is complex). To these multiplication times must be added the time required for the pivot search, if any. Pivot searching is done to minimize round-off error as discussed by Fox [18] and Wilkinson [19].

In Chao and Strait's [17] program the linear system for current distribution is solved by inversion. Unless the current distribution for many different excitations of the same antenna at the same frequency must be calculated, solution of the system by Gauss elimination as suggested by Fox [18] is about three times faster than by inversion, not counting the time spent in the pivot search.

Pivot selection is usually done by either of two methods. The first method, partial pivoting, involves searching the pivot column for an appropriate pivot element. In the second method, complete pivoting, all elements below and to the right of the last pivot element are examined in the search for the next pivot element. In most pivot selection schemes the element with largest modulus is chosen as pivot. With real numbers the modulus is just the absolute value of an element, which can be evaluated very quickly. With complex numbers, however, the evaluation of the modulus of an element is much slower. For example the IBM 360/65 computer can evaluate an absolute value in less than one microsecond, while determining the modulus of a complex number requires over one hundred microseconds, using the CABS function in FORTRAN as noted in [20].

To illustrate the possible significance of pivot search time, consider subroutine LINEQ given by Chao and Strait [17]. This routine looks much like IBM's MINV matrix inversion routine, modified for complex numbers. When LINEQ is used on the 360/65, the evaluation of CABS in the pivot search consumes as much time as the rest of the inversion process. A similar situation exists in the case of CGELG, a Gauss elimination routine available at the Iowa State University Computation Center. This complex pivoting routine also spends about as much time evaluating CABS in the pivot search as is needed to solve the system.

Another possible pivot selection scheme involves choosing the element with greatest norm as pivot, where the norm used is the sum of the absolute value of the real plus the absolute value of the imaginary parts of the element. While this scheme usually results in use of a different pivot element than would be used when the modulus is evaluated, it should be noted that the modulus of the pivot element chosen by this norm scheme is never smaller than $\sqrt{2}/2$ times the modulus of the pivot element when selected for largest modulus. Extensive numerical examples were run which showed that use of this norm pivot selection scheme yielded accuracy comparable to that obtained using the time consuming modulus evaluation. Numerical examples showed that Chao and Strait's [17] complex matrix inversion routine LINEQ could be executed twice as fast using the norm pivot selection scheme as compared to the modulus scheme.

After trying several methods to solve the linear system for the current distribution, it was concluded that Gauss elimination with partial pivoting using the norm pivot selection scheme suggested here should be used in the numerical solution of the NMHD because of the speed with which this method could solve the system. Numerical experiments indicated that for the systems solved here the accuracy of this method was similar to that obtained using a Gauss elimination routine with complete pivoting where the pivot was determined on the basis of modulus. The partial pivoting Gauss elimination routine used is subroutine SGEA listed in the Appendix. Note that this routine solves the linear system for current distribution about six times faster than LINEQ and about two and one-half times faster than CGELG. Note also that since the program developed here accounts for symmetry, the current distribution can be calculated about forty-eight times faster than would be possible using the program of Chao and Strait [17]. Since the numerical work done here required several hundred dollars worth of computer time, it is clear that the factor of forty-eight is quite significant.

Since the NMHD in its second resonance is not a very efficient antenna, as noted by Stephenson and Mayes [6], the determination of radiation efficiency for the NMHD is an important part of this work. The program of Chao and Strait [17] does not calculate radiation efficiency. Weeks [21] defines radiation efficiency to be the ratio of the radiated power to the input power. The input power and the radiated power differ by the power dissipated by the antenna. The dissipated power is due to the ohmic loss of the copper wire. In order to account for the finite conductivity of copper, the a.c. resistance of each segment is calculated in the program developed here. Then the linear system to be solved for current distribution is modified to account for this a.c. resistance. After the current distribution has been found, the ohmic loss for each segment is calculated. The dissipated power is just the sum of these ohmic losses. The radiation efficiency is then easily obtained.

Due to computational considerations, bandwidth is calculated from an equivalent circuit model for the antenna. The input impedance for the antenna is calculated for two frequencies near resonance, and then a series R, L, C circuit model is determined for the antenna as suggested by Jordan and Balmain [22]. The bandwidth of the antenna is then defined to be the bandwidth of this series model. Bandwidths calculated in this way gave close agreement with those found by calculating the input impedance of the antenna at many frequencies. Calculated bandwidths of a few tenths of one percent are found to give close agreement with those measured by Stephenson and Mayes [6] and Lain, Ziolkowski, and Mayes [7] for the NMHD in its second resonance.

The computer program listed in the Appendix is suitable for numerical investigation of the characteristics of the NMHD. Current distribution, input impedance, radiation resistance, efficiency, and directive gain can be determined with this program. The numerical results given are found to agree reasonably well with the experimental work of Stephenson and Mayes [6] and also that of Lain, Ziolkowski, and Mayes [7].

II. NUMERICAL METHOD

The electric field $\overline{E}^s$ scattered from a conductor placed in an impressed field $\overline{E}^i$ is given by Harrington [23] as

$$\overline{E}^s = -j\omega\overline{A} - \overline{\nabla}\Phi \tag{1}$$

where

$$\overline{A} = \mu \oint\!\!\oint_s \frac{\overline{J}e^{-jkR}}{4\pi R}\, ds \tag{2}$$

$$\Phi = \frac{1}{\epsilon} \oint\!\!\oint_s \frac{\sigma e^{-jkR}}{4\pi R}\, ds \tag{3}$$

$$\sigma = -\frac{1}{j\omega}\,\overline{\nabla}\cdot\overline{J} \tag{4}$$

with angular frequency ω, vector magnetic potential $\overline{A}$, scalar electric potential Φ, permeability μ, surface current density $\overline{J}$, propagation constant k, permittivity ϵ, surface charge density σ, and the distance from a source point on the surface s of the conductor to the field point is denoted by R. The boundary condition that tangential electric field be zero at the conductor surface is accounted for by

$$\hat{n} \times \overline{E}^s = -\hat{n} \times \overline{E}^i \tag{5}$$

at the conductor surface where $\hat{n}$ is the unit vector normal to the surface of the conductor.

If the conductor is a thin wire with length much greater than radius, and radius much less than a wavelength at the frequency of interest, we assume

i) current flows along the axis of the wire

ii) current and charge densities are filaments of current I and charge σ on the wire axis

iii) $\hat{n} \times \overline{E}^s = -\hat{n} \times \overline{E}^i$ is applied only to the axial component of $\overline{E}$ at the surface of the conductor.

Under these assumptions we can write

$$- E_{\ell}^{i} = -j\omega A_{\ell} - \frac{\partial \Phi}{\partial \ell} \tag{6}$$

at the surface of the wire, and

$$\overline{A} = \mu \int_{\Gamma} \frac{\overline{I}(\ell) e^{-jkR}}{4\pi R} \, d\ell \tag{7}$$

$$\Phi = \frac{1}{\epsilon} \int_{\Gamma} \frac{\sigma(\ell) e^{-jkR}}{4\pi R} \, d\ell \tag{8}$$

$$\sigma = -\frac{1}{j\omega} \frac{dI}{d\ell} \tag{9}$$

where ℓ is the length variable along the wire axis and Γ denotes the path traced out by the wire axis.

The axis of the wire is divided into N segments with the n^{th} segment denoted by starting point n^-, midpoint n, and termination point n^+, as shown in Figure 1. The boundary condition that the current is zero at the ends of the wire is accounted for by the extra half segment at each end of the wire, as shown in Figure 1. The integrals of (7) and (8) are approximated by summations and the derivatives of (6) and (9) are approximated by finite differences as discussed by Henrici [24] and

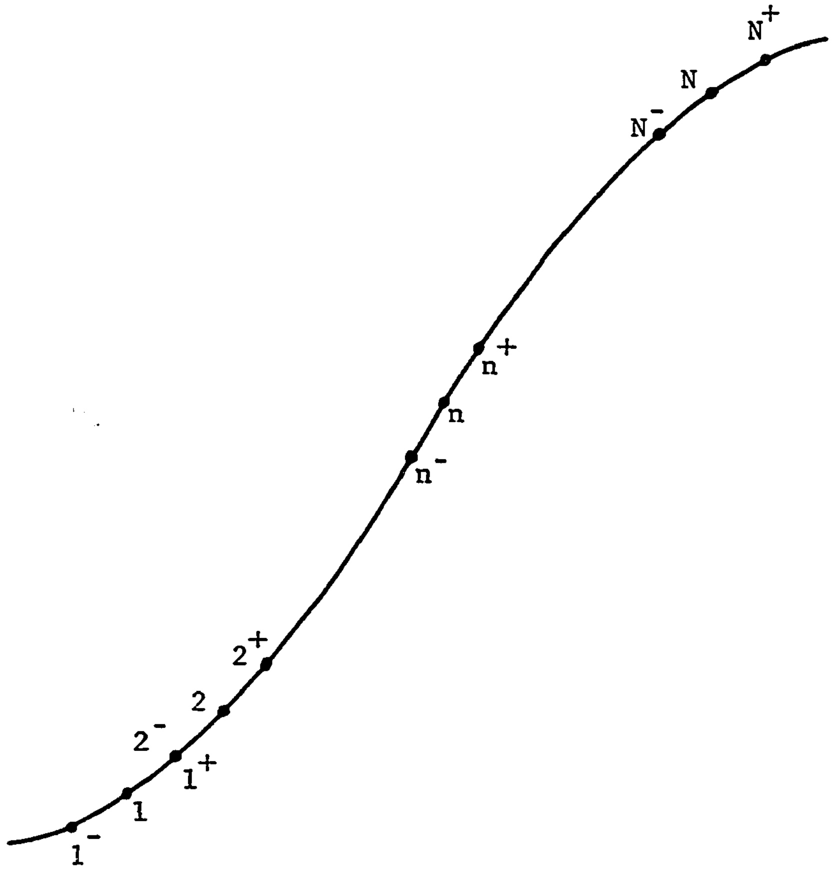

Figure 1. Wire axis divided into N segments

Varga [25]. With these approximations (6), (7), (8), and (9) can be written in the form

$$- E^i_\ell(m) \approx -j\omega A_\ell(m) - \frac{\Phi(m^+) - \Phi(m^-)}{\Delta \ell_m} \tag{10}$$

at the surface of the wire, and

$$\bar{A}(m) \approx \mu \sum_{n=1}^{N} \bar{I}(n) \int_{\Delta\ell_n} \frac{e^{-jkR}}{4\pi R}\, d\ell \tag{11}$$

$$\Phi(m^+) \approx \frac{1}{\epsilon} \sum_{n=1}^{N} \sigma(n^+) \int_{\Delta\ell_{n^+}} \frac{e^{-jkR}}{4\pi R}\, d\ell \tag{12}$$

$$\Phi(m^-) \approx \frac{1}{\epsilon} \sum_{n=1}^{N} \sigma(n^-) \int_{\Delta\ell_{n^-}} \frac{e^{-jkR}}{4\pi R}\, d\ell \tag{13}$$

$$\sigma(n^+) \approx - \frac{1}{j\omega} \left[\frac{I(n+1) - I(n)}{\Delta\ell_{n^+}}\right] \tag{14}$$

$$\sigma(n^-) \approx - \frac{1}{j\omega} \left[\frac{I(n) - I(n-1)}{\Delta\ell_{n^-}}\right] \tag{15}$$

where $\Delta\ell_n$, $\Delta\ell_{n^+}$, and $\Delta\ell_{n^-}$ are the lengths of the segments from n^- to n^+, from n to n+1, and from n-1 to n, respectively. Since the σ's are given in terms of a linear combination of the I's by (14) and (15), clearly the Φ's of (12) and (13) can also be expressed as a linear combination of the I's, as can $\bar{A}$ in (11). Thus $-\bar{E}^i(m)$ can be expressed as a linear combination of the I's.

Let

$$[I] = \begin{bmatrix} I(1) \\ I(2) \\ \cdot \\ \cdot \\ I(N) \end{bmatrix}, \quad \text{and} \quad [V] = \begin{bmatrix} \bar{E}^{i}(1) \cdot \overline{\Delta\ell}_1 \\ \bar{E}^{i}(2) \cdot \overline{\Delta\ell}_2 \\ \cdot \\ \cdot \\ \bar{E}^{i}(N) \cdot \overline{\Delta\ell}_N \end{bmatrix} \tag{16}$$

Since $E^{i}_{\ell}(m)\Delta\ell_m = \bar{E}^{i}(m)\cdot\overline{\Delta\ell}_m$ is a linear combination of the I's, we can write

$$[V] = [Z][I] \tag{17}$$

where the elements of [Z] can be obtained by rearranging (10) through (15) into the form of (17). Note that an arbitrary element of [Z] is given by

$$Z_{mn} = \bar{E}^{i}(m)\Big|_{\substack{\text{"due to} \\ I(n)\text{"}}} \cdot \overline{\Delta\ell}_m / I(n) \tag{18}$$

where

$$\bar{E}^{i}(m)\Big|_{\substack{\text{"due to} \\ I(n)\text{"}}} = -\bar{E}^{s}(m)\Big|_{\substack{\text{due to} \\ I(n)}} \quad \text{on s.} \tag{19}$$

In a typical antenna problem the elements of [V] and the geometry of the wire axis are known, while the current distribution [I] is unknown. If the elements of [Z] can be calculated from the geometry, then the current distribution can be obtained by solving the linear system of (17). In the computer programs of Strait and Hirasawa [16] and of Chao and Strait [17], the inverse of [Z] is calculated and then the current distribution is found using

$$[I] = [Z]^{-1}[V] \tag{20}$$

Unless the current distribution for many different excitations [V] of the same antenna at the same frequency must be determined, solution of the linear system of (17) by Gauss elimination or one of the equivalent methods, is faster than forming the inverse of [Z]. For large systems (17) can be solved approximately three times faster by Gauss elimination than by the corresponding inversion method as noted by Fox [18].

The integrals in (11), (12), and (13) are of the same form and will be denoted by

$$\psi(m,n) = \frac{1}{4\pi\Delta\ell_n}\int_{\Delta\ell_n} \frac{e^{-jkR_{mn}(\zeta')}}{R_{mn}(\zeta')}\,d\zeta' \tag{21}$$

where $R_{mn}(\zeta')$ is the distance between the point m and a source point on the n^{th} segment as shown in Figure 2. Similarly,

$$\psi(m^+,n^+) = \frac{1}{4\pi\Delta\ell_{n^+}}\int_{\Delta\ell_{n^+}} \frac{e^{-jkR_{m^+n^+}(\zeta')}}{R_{m^+n^+}(\zeta')}\,d\zeta' \tag{22}$$

where $R_{m^+n^+}(\zeta')$ is the distance between the point m and a source point on $\Delta\ell_{n^+}$. Expressions for $\psi(m^-,n^-)$, $\psi(m^-,n^+)$, and $\psi(m^+,n^-)$ follow directly. The evaluation of these ψ integrals will be considered later.

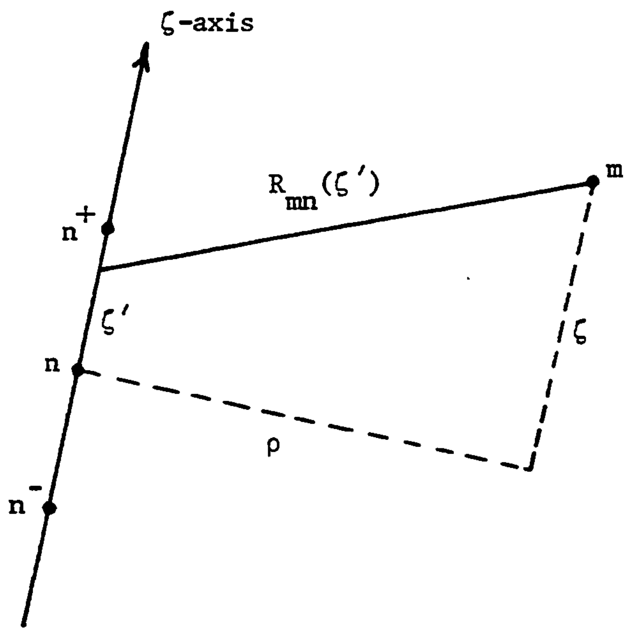

Figure 2. Local cylindrical coordinate system

Let the n^{th} segment be represented by a current filament I(n) and two filaments of net charge

$$q(n^+) = \frac{1}{j\omega} I(n), \quad q(n^-) = -\frac{1}{j\omega} I(n) \tag{23}$$

where $q = \sigma\Delta\ell$. The vector potential at m due to I(n) is, by (11),

$$\left.\bar{A}(m)\right|_{\substack{\text{due to}\\ I(n)}} = \mu\, I(n)\, \overline{\Delta\ell}_n\, \psi(m,n) \tag{24}$$

The scalar potentials at m^+ and m^- due to the charges of (23) are, by (12) and (13),

$$\left.\Phi(m^+)\right|_{\substack{\text{due to}\\ q(n^+)}} = \frac{q(n^+)}{\epsilon}\, \psi(m^+,n^+) \tag{25}$$

$$\left.\Phi(m^+)\right|_{\substack{\text{due to}\\ q(n^-)}} = \frac{q(n^-)}{\epsilon}\, \psi(m^+,n^-) \tag{26}$$

$$\left.\Phi(m^-)\right|_{\substack{\text{due to}\\ q(n^+)}} = \frac{q(n^+)}{\epsilon}\, \psi(m^-,n^+) \tag{27}$$

$$\left.\Phi(m^-)\right|_{\substack{\text{due to}\\ q(n^-)}} = \frac{q(n^-)}{\epsilon}\, \psi(m^-,n^-) \tag{28}$$

The substitution of (23) into (25) through (28) gives

$$\Phi(m^+)\Big|_{\substack{\text{due to } n^{th}\\ \text{segment}}} = \frac{1}{j\omega\epsilon} I(n)[\psi(m^+,n^+) - \psi(m^+,n^-)] \tag{29}$$

$$\Phi(m^-)\Big|_{\substack{\text{due to } n^{th}\\ \text{segment}}} = \frac{1}{j\omega\epsilon} I(n)[\psi m^-,n^+) - \psi(m^-,n^-)] \tag{30}$$

Now the substitution of (24), (29), and (30) into (10) gives

$$E_\ell^i(m)\Big|_{\substack{\text{"due to}\\ I(n)\text{"}}} = j\omega\mu\, I(n) \frac{\overline{\Delta\ell}_m \cdot \overline{\Delta\ell}_n}{\Delta\ell_m} \psi(m,n) + \frac{I(n)}{j\omega\epsilon\Delta\ell_m} [\psi(m^+,n^+) - \psi(m^+,n^-) - \psi(m^-,n^+) + \psi(m^-,n^-)] \tag{31}$$

at the conductor surface.

Note that

$$\overline{E}^i(m)\Big|_{\substack{\text{"due to}\\ I(n)\text{"}}} \cdot \overline{\Delta\ell}_m = E_\ell^i(m)\Delta\ell_m\Big|_{\substack{\text{"due to}\\ I(n)\text{"}}} \tag{32}$$

The substitution of (32) into (31) gives

$$\overline{E}^i(m)\Big|_{\substack{\text{"due to}\\ I(n)\text{"}}} \cdot \overline{\Delta\ell}_m = j\omega\mu\, I(n)\, \overline{\Delta\ell}_m \cdot \overline{\Delta\ell}_n\, \psi(m,n) + \frac{I(n)}{j\omega\epsilon} [\psi(m^+,n^+) - \psi(m^+,n^-) - \psi(m^-,n^+) + \psi(m^-,n^-)] \tag{33}$$

Now the elements of [Z] can be found by substituting (33) into (18) which gives

$$Z_{mn} = j\omega\mu\,\overline{\Delta\ell}_m \cdot \overline{\Delta\ell}_n \psi(m,n) + \frac{1}{j\omega\epsilon}\left[\psi(m^+,n^+) - \psi(m^+,n^-) - \psi(n^-,n^+) + \psi(m^-,n^-)\right] \qquad (34)$$

Since $\overline{\Delta\ell}_m \cdot \overline{\Delta\ell}_n$ is easily obtained from the geometry, all that remains to be done is the evaluation of the ψ integrals and then each element of [Z] can be calculated.

Recall that

$$\psi(m,n) = \frac{1}{4\pi\Delta\ell_n}\int_{\Delta\ell_n} \frac{e^{-jkR_{mn}(\zeta')}}{R_{mn}(\zeta')}\,d\zeta' \qquad (21)$$

where ζ' is some integration point along the ζ-axis of a cylindrical coordinate frame in which the ζ-axis is tangent to element $\Delta\ell_n$ at its midpoint n as shown in Figure 2.

Harrington [13] suggests that $R_{mn}(\zeta')$ be approximated by

$$R_{mn}(\zeta') \approx \begin{cases} \sqrt{\rho^2 + (\zeta-\zeta')^2}, & m \neq n \\ \sqrt{a^2 + (\zeta')^2}, & m = n \end{cases} \qquad (35)$$

where a is the radius of the wire. Let $\alpha = \Delta\ell_n/2$. Then (21) can be written in the form

$$\psi(m,n) = \frac{1}{8\pi\alpha}\int_{-\alpha}^{\alpha} \frac{e^{-jkR_{mn}(\zeta')}}{R_{mn}(\zeta')}\,d\zeta' \qquad (36)$$

Harrington [13] gives formulas for evaluating (36) based on five-term Maclaurin expansions for the Green's function. One formula is developed which converges well for small R, that is for $R < 10\alpha$, and another is given which converges well for $R \geq 10\alpha$. These formulas were used in the programs of Strait and Hirasawa [16] and Chao and Strait [17] and are also used here in subroutine CAZZ listed in the Appendix.

Losses due to the finite conductivity of the wire can easily be accounted for. At high frequencies the resistance of each segment is due to the skin effect, as discussed by Hayt [26] and by Adler, Chu, and Fano [27]. The resistance per segment can be calculated using the formulas given in the popular ITT handbook [28]. This resistance must be added to the self-impedance of each element, that is, to the diagonal elements of [Z], before the linear system of (17) is solved.

In order to calculate the radiated (scattered) field, an appropriate numerical formula must be formed. Recall that the scattered field is given by

$$\overline{E}^{s} = -j\omega\overline{A} - \overline{\nabla}\Phi \tag{1}$$

For a field point remote from the antenna (a point in the far-field) the scalar potential need not be considered since it does not contribute to the far-field of the antenna. It is convenient to work in the spherical coordinate system of Figure 3. Since only the θ and ϕ components of $\overline{E}^{s}$ contribute to the radiation field, all that must be evaluated is

$$E_{\theta}^{s}(\overline{r}) = -j\omega A_{\theta}(\overline{r}) \tag{37}$$

$$E_{\phi}^{s}(\overline{r}) = -j\omega A_{\phi}(\overline{r}) \tag{38}$$

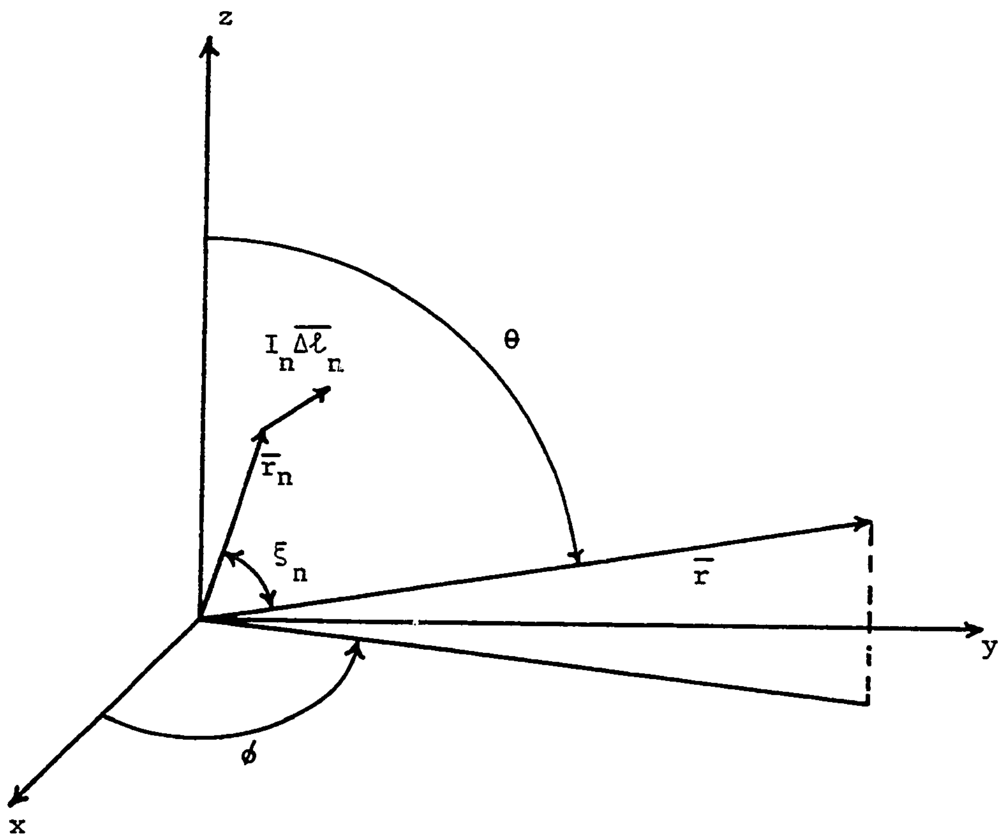

Figure 3. Spherical coordinate system for evaluation of vector potential $\overline{A}(\overline{r})$

where $|\bar{r}|$ is sufficiently large that the field point is indeed in the far-field.

The vector magnetic potential due to a filament of current is known to be

$$\bar{A}(\bar{r}) = \frac{\mu}{4\pi}\int_{\Gamma} \frac{I(\bar{r}')\overline{d\ell}' e^{-jk|\bar{r} - \bar{r}'|}}{|\bar{r} - \bar{r}'|} \tag{39}$$

where $\bar{r}$ denotes the field point, $\bar{r}'$ denotes a source point on the filament, and Γ is the path traced out by the filament. This integral may be evaluated numerically using

$$\bar{A}(\bar{r}) \approx \frac{\mu}{4\pi} \sum_{n=1}^{N} \frac{I_n \overline{\Delta\ell}_n e^{-jk|\bar{r} - \bar{r}_n|}}{|\bar{r} - \bar{r}_n|} \tag{40}$$

where $I_n \overline{\Delta\ell}_n$ is the current element along the n^{th} segment located by position vector $\bar{r}_n$. For $|\bar{r}| \gg |\bar{r}_n|$, this integral can be written as

$$\bar{A}(\bar{r}) \approx \frac{\mu}{4\pi} \sum_{n=1}^{N} \frac{I_n \overline{\Delta\ell}_n e^{-jk|\bar{r} - \bar{r}_n|}}{|\bar{r}|} \tag{41}$$

Note that $\bar{r}_n$ cannot be neglected in the phase expression.

Now for $|\bar{r}| \gg |\bar{r}_n|$ we have

$$|\bar{r} - \bar{r}_n| \approx |\bar{r}| - |\bar{r}_n| \cos \xi_n = r_o - r_n \cos \xi_n \tag{42}$$

where ξ_n is the angle between $\bar{r}$ and $\bar{r}_n$ as shown in Figure 3. Finally, the vector field may be calculated using

$$\bar{A}(\bar{r}) \approx \frac{\mu e^{-jkr_o}}{4\pi r_o} \sum_{n=1}^{N} I_n \overline{\Delta\ell}_n e^{jkr_n \cos\xi_n} \qquad (43)$$

and (43) can be substituted into (37) and (38) to find the far-field.

III. APPLICATION OF THE NUMERICAL METHOD TO THE NMHD

In order to apply the matrix method of Harrington [13] to the NMHD, it is necessary to first examine the geometry of the NMHD. The wire axis of a NMHD is shown in Figure 4. This helix is characterized by mean diameter D, pitch p, and halflength h. The pitch angle γ is given by

$$\gamma = \tan^{-1} \frac{p}{\pi D} \tag{44}$$

The axis of the helix is assumed to lie along the z-axis with the feed point (midpoint) at $x = 0$, $y = D/2$, $z = 0$. The axis of the wire lies along the helix characterized by the parametric equations

$$x = -\frac{D}{2} \sin\left(\frac{2\pi z}{p}\right) \tag{45}$$

$$y = \frac{D}{2} \cos\left(\frac{2\pi z}{p}\right) \tag{46}$$

where $-h \le z \le h$. The wire radius is denoted by a.

The axis of the wire is divided into N equal length segments (plus two half-segments at the wire ends) where N is odd. The segments are numbered consecutively from one to N, from the segment with most negative z-component to that with most positive z-component, respectively. Note that the feed point is at the $(N+1)/2$ th segment. Each segment n has a beginning point n^-, a midpoint n, and a termination point n^+. Let $z^-(n)$, $z(n)$, and $z^+(n)$ denote the z-coordinate of n^-, n, and n^+, respectively. Clearly we can write

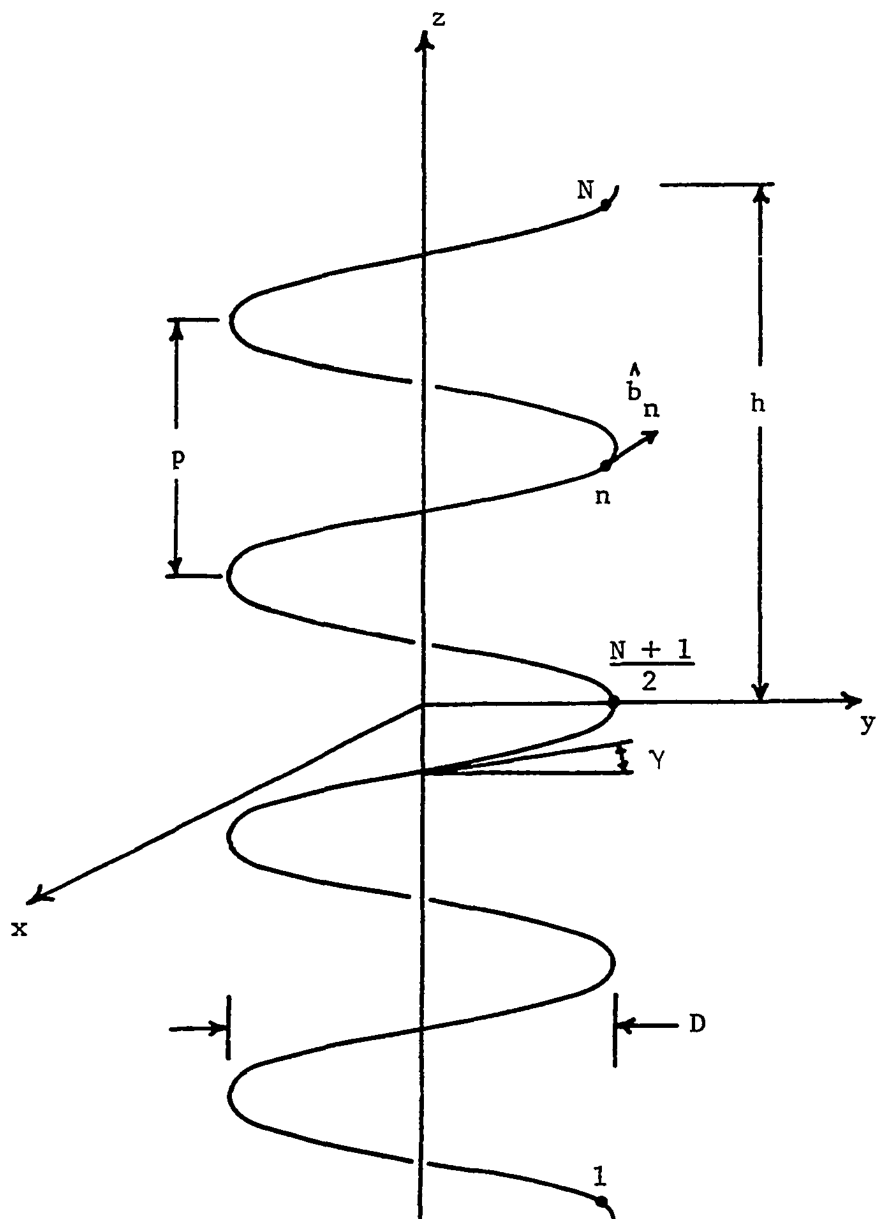

Figure 4. Geometry of a normal mode helical dipole

$$z(n) = \Delta z(n - \frac{N+1}{2}) \tag{47}$$

$$z^-(n) = z(n) - \frac{\Delta z}{2} \tag{48}$$

$$z^+(n) = z(n) + \frac{\Delta z}{2} \tag{49}$$

where $\Delta z = 2h/(N + 1)$ is the length of the projection of one segment onto the z-axis. The x and y coordinates of points n, n^-, and n^+ can easily be found by the substitution of (47), (48), and (49) into (45) and (46).

Let $\Delta\ell$ denote the length of each segment. This length can be evaluated using the line integral

$$\Delta\ell = \underset{\text{along helix}}{\int_0^{\Delta z}} [(\frac{dx}{dz})^2 + (\frac{dy}{dz})^2 + 1]^{\frac{1}{2}} dz \tag{50}$$

When (45) and (46) are substituted into (50), the result is

$$\Delta\ell = \Delta z[(\frac{D\pi}{p})^2 + 1]^{\frac{1}{2}} \tag{51}$$

In addition to the coordinates describing the helix, unit vectors pointing along the helix are needed at all points n^-, n, and n^+. Let $\hat{b}(n^-)$, $\hat{b}(n)$, and $\hat{b}(n^+)$ denote unit vectors along the wire axis at the points n^-, n, and n^+, respectively. It is clear that

$$\hat{b}(n) = -\hat{a}_x \cos\gamma \cos[\frac{2\pi z(n)}{p}] - \hat{a}_y \cos\gamma \sin[\frac{2\pi z(n)}{p}] + \hat{a}_z \sin\gamma \tag{52}$$

with similar expressions for $\hat{b}(n^-)$ and $\hat{b}(n^+)$, where $\hat{a}_x$, $\hat{a}_y$, and $\hat{a}_z$ are unit vectors along the x, y, and z axis respectively, of Figure 4.

An arbitrary element of [Z] as given by (34) can be written in the form

$$Z_{mn} = j\omega\mu \ell^2 \hat{b}_m \cdot \hat{b}_n \psi(m,n)$$

$$+ \frac{1}{j\omega\epsilon} [\psi(m^+,n^+) - \psi(m^+,n^-) - \psi(m^-,n^+) + \psi(m^-,n^-)] \qquad (53)$$

where

$$\psi(m,n) = \frac{1}{4\pi\ell} \int_\ell \frac{e^{-jkR_{mn}(\zeta')}}{R_{mn}(\zeta')} d\zeta' \qquad (54)$$

For the geometry considered here, $\psi(m,n) = \psi(m^-,n^-) = \psi(m^+,n^+)$, $\psi(m^-,n^+) = \psi(m,n+1)$, and $\psi(m^+,n^-) = \psi(m,n-1)$. Thus (53) can be written as

$$Z_{mn} = j\omega\mu \ell^2 \hat{b}_m \cdot \hat{b}_n \psi(m,n) + \frac{1}{j\omega\epsilon} [2\psi(m,n) - \psi(m,n+1) - \psi(m,n-1)] \qquad (55)$$

Note that from the geometry it is obvious that the N^2 elements of [Z] can be written in terms of N distinct elements Z_r, such that

$$Z_{mn} = Z_r \qquad (56)$$

where $r = |m - n| + 1$. Thus we can write

$$[Z] = \begin{bmatrix} Z_1 & Z_2 & \cdots & Z_N \\ Z_2 & Z_1 & \cdots & \\ \vdots & & \ddots & \\ Z_N & & & Z_1 \end{bmatrix} \qquad (57)$$

In a similar manner we can write

$$\psi(m,n) = \psi_r \tag{58}$$

where the ψ_r's form the sequence $\{\psi_r : \psi_1, \psi_2, \ldots, \psi_N, \psi_{N+1}\}$ and $\psi_1 = \psi(m,m)$ and $\psi_{N+1} = \psi(1^-, N^+)$. Thus (55) can be written as

$$Z_{|m-n|+1} = j\omega\mu \ell^2 \hat{b}_m \cdot \hat{b}_n \psi_{|m-n|+1} + \frac{1}{j\omega\epsilon}\left[2\psi_{|m-n|+1} - \psi_{|m-n-1|+1} - \psi_{|m-n+1|+1}\right] \tag{59}$$

This can be expressed in the form

$$Z_r = j\omega\mu\ell^2 B_r \psi_r + \begin{cases} \frac{1}{j\omega\epsilon}\left[2\psi_r - 2\psi_{r+1}\right] & , \ r = 1 \\ \frac{1}{j\omega\epsilon}\left[2\psi_r - \psi_{r-1} - \psi_{r+1}\right], & r \neq 1 \end{cases} \tag{60}$$

where $B_r = \hat{b}_1 \cdot \hat{b}_{1+r}$. The Z's of (60) are calculated in subroutine CAZZ, listed in the Appendix. The ψ's are evaluated in this routine using the formulas given by Harrington [13].

Now the problem symmetry must be considered. Recall that the linear system to be solved for current distribution is of the form

$$[Z][I] = [V] \tag{61}$$

where $[Z]$ is N by N (N odd) and $[V]$ and $[I]$ are both N-element column vectors. For the NMHD considered here, the excitation is assumed to be a unit amplitude voltage generator located at the midpoint of the antenna. Under this assumption the elements of [V] are all zero, except for the (N+1)/2 th element, which is unity. Due to the symmetry of [Z] and [V], [I] will have the form

$$[I] = \begin{bmatrix} I_1 \\ I_2 \\ \vdots \\ I_{\frac{N+1}{2}} \\ \vdots \\ I_2 \\ I_1 \end{bmatrix} \tag{62}$$

Now the linear system can be written out as

$$\begin{bmatrix} Z_1 & Z_2 & \cdots & Z_N \\ Z_2 & Z_1 & & \\ \vdots & & \ddots & \\ Z_N & & & Z_1 \end{bmatrix} \begin{bmatrix} I_1 \\ I_2 \\ \vdots \\ I_{\frac{N+1}{2}} \\ \vdots \\ I_2 \\ I_1 \end{bmatrix} = \begin{bmatrix} 0 \\ 0 \\ \vdots \\ 1 \\ \vdots \\ 0 \\ 0 \end{bmatrix} \tag{63}$$

Define permutation matrix [J] such that

$$[J] = \begin{bmatrix} 0 & & 1 \\ & \cdot^{\cdot^{\cdot}} & \\ 1 & & 0 \end{bmatrix} \tag{64}$$

Clearly the system of (63) can be written in partitioned form as

$$\begin{bmatrix} A & \bar{a} & B \\ \bar{a}^T & c & \bar{a}^T J \\ B^T & J\bar{a} & A \end{bmatrix} \begin{bmatrix} \bar{d} \\ e \\ J\bar{d} \end{bmatrix} = \begin{bmatrix} \bar{0} \\ 1 \\ \bar{0} \end{bmatrix} \tag{65}$$

where A, B, and J are (N+1)/2 by (N+1)/2 matrices, $\bar{a}$, $\bar{d}$, and $\bar{0}$ are (N+1)/2 element column vectors, and c, e, and 1 are scalar quantities. Note that superscript T denotes transpose. Multiplying out (65) gives

$$A\bar{d} + \bar{a}e + BJ\bar{d} = \bar{0} \tag{66}$$

$$\bar{a}^T\bar{d} + ce + a^T JJ\bar{d} = 1 \tag{67}$$

$$B^T\bar{d} + J\bar{a}e + AJ\bar{d} = \bar{0} \tag{68}$$

The equivalence of (66) and (68) can be shown by premultiplying both sides of (68) by J to give

$$JB^T\bar{d} + \bar{a}e + JAJ\bar{d} = \bar{0} \tag{69}$$

Note that JJ = I, the identity matrix, JAJ = A, and JBJ = B^T. Clearly then, BJ = JB^T and the equivalence of (66) and (68) is shown.

A reduced system of linear equations which can be solved for the current distribution can be formed from (66) and (67), such that

$$\begin{bmatrix} A + BJ & \bar{a} \\ 2\bar{a}^T & c \end{bmatrix} \begin{bmatrix} \bar{d} \\ e \end{bmatrix} = \begin{bmatrix} \bar{0} \\ 1 \end{bmatrix} \tag{70}$$

This reduced system has order (N+1)/2. The elements of the coefficient matrix for the reduced system are just linear combinations of the Z_r's of (60) and are easily found. Subroutine CAZR, listed in the Appendix, forms this coefficient matrix. Note that BJ is merely a resubscripting process which can be accomplished very quickly.

The effect of finite wire conductivity is accounted for by adding the a.c. resistance per segment to Z_1, that is, to the self impedance of each segment.

The linear system of (70) is solved for the NMHD current distribution using subroutine SGEA, listed in the Appendix. This is a Gauss elimination algorithm, as previously noted. In order to check the accuracy of the solution, subroutine VCHK is used. In this subroutine the calculated current distribution is used in (70) and the corresponding excitation is calculated. A comparison of this with the assumed excitation can then be made.

In order to calculate the directive gain of the NMHD, the total radiated power as well as the radiated fields must be calculated. The radiated fields are easily determined using (43), (37), and (38). In principle the total radiated power could be obtained by integrating the radiated power density over a sphere surrounding the antenna. It is simpler, however, to note that the radiated power equals the input power minus the dissipated power. The input power P_{in} is just

$$P_{in} = \tfrac{1}{2}\,\mathrm{Re}\,(VI^*) \tag{71}$$

where V is the amplitude of the source voltage and I^* is the complex conjugate of the antenna current at the midpoint. The power dissipated P_{diss} can be found by summing the ohmic losses due to the a.c. resistance of each segment. Thus

$$P_{diss} = \frac{R_s}{2} \sum_{n=1}^{N} |I(n)|^2 \tag{72}$$

where R_s is the a.c. resistance per segment. The radiated power is

$$P_{rad} = P_{in} - P_{diss} \tag{73}$$

Since the radiation field of the NMHD contains both the θ and the ϕ components of electric field, and a comparison of each component is of interest, directive gains for each component are defined such that

$$G_\theta(r,\theta,\phi) = \frac{\frac{1}{2\eta} |E_\theta(r,\theta,\phi)|^2}{S_o} \tag{74}$$

$$G_\phi(r,\theta,\phi) = \frac{\frac{1}{2\eta} |E_\phi(r,\theta,\phi)|^2}{S_o} \tag{75}$$

where $S_o = P_{rad}/(4\pi r^2)$ and r is the distance from the antenna to the far-field point of interest and η is the intrinsic impedance of free space. Subroutines CORD and GAIND are used to calculate these directive gains for the NMHD.

IV. NUMERICAL RESULTS

The numerical method was applied to five NMHD's for both the first and second resonances. Each antenna consisted of twenty-five turns of A. W. G. number twelve copper wire. The axial halflength and the pitch of each helix was fixed at twenty-five centimeters and two centimeters, respectively. Only the diameter of the helix was varied in these numerical experiments. The dimensions of the antennas are given in Table 1.

Table 1. Helix dimensions

Antenna designation	Halflength cm.	Pitch cm.	Diameter cm.	Pitch angle γ degrees
HD - 10A	25	2	2.0	17.66
HD - 13A	25	2	2.6	13.76
HD - 16A	25	2	3.2	11.25
HD - 18A	25	2	3.6	10.03
HD - 20A	25	2	4.0	9.04

The antennas of Table 1 were each approximated by two hundred fifty-one segments, plus the extra half-segment at each end. Thus each turn of the helix was represented by about ten segments. The results of the numerical analysis of these antennas in the first and second resonances are summarized in Tables 2 and 3, respectively. The results include the free space resonant wavelength λ_o, shortening factor s ($s = 4h/\lambda_o$ for the first resonance and $s = 4h/(3\lambda_o)$ for the second resonance), input

Table 2. Summary of numerical results for first resonance

Antenna designation	λ_o meters	Shortening factor s	R_{in} ohms	R_{rad} ohms	Efficiency %	Bandwidth %	Directivity θ-component
HD - 10A	1.8205	0.5493	27.73	27.26	98.3	6.62	1.542
HD - 13A	2.2071	0.4531	19.65	19.10	97.2	4.08	1.523
HD - 16A	2.6508	0.3772	14.20	13.58	95.7	2.71	1.508
HD - 18A	2.9768	0.3359	11.60	10.94	94.3	2.10	1.499
HD - 20A	3.3225	0.3010	9.61	8.91	92.8	1.50	1.492

Table 3. Summary of numerical results for second resonance

Antenna designation	λ_o meters	Shortening factor s	R_{in} ohms	R_{rad} ohms	Efficiency %	Bandwidth %	Directivity θ-component
HD - 10A	0.6473	0.5150	9.95	9.22	92.7	1.06	2.853
HD - 13A	0.8131	0.4100	6.70	5.88	87.8	0.68	2.614
HD - 16A	1.0040	0.3320	5.10	4.20	82.4	0.50	2.279
HD - 18A	1.1434	0.2915	4.44	3.50	78.8	0.45	2.060
HD - 20A	1.2915	0.2581	3.93	2.94	75.0	0.42	1.889

resistance R_{in} at resonance, radiation resistance R_{rad} at resonance, radiation efficiency, percent bandwidth, and directivity or maximum directive gain for the θ component of the far-field.

The results are presented graphically in Figures 5 through 9. The sidelobe level in the second resonance is shown in Figure 10. The measurements by Lain, Ziolkowski, and Mayes [7] of some of these characteristics for the second resonance are included on the appropriate figures for comparison. Stephenson and Mayes' [6] calculated directivity, based on an assumed sinusoidal current distribution, is included on Figure 8 for comparison.

For each resonance of each antenna a numerical solution was found at two wavelengths near resonance. By linear interpolation of the input reactance calculated at these two wavelengths, a good approximation to the resonant wavelength was obtained. The input resistance, radiation resistance, efficiency, and directivity at resonance were also found by linear interpolation. The slope of the input reactance near resonance and the input resistance at resonance were then used to obtain a R, L, C series equivalent circuit for the NMHD near resonance. The bandwidth of the NMHD was then defined to be the bandwidth of this equivalent circuit. Bandwidth was determined in this manner in order to reduce the total amount of computer time used. In preliminary numerical experiments in which the helices were approximated by one hundred fifty-one segments, bandwidth determined from the equivalent circuit was found to agree very closely with bandwidth obtained by extensive numerical experiments, where the latter bandwidth was defined to be the range of frequency over which the input reactance was less than the input resistance at resonance.

The numerical results also include the current distribution $I = |I|\angle\phi$ along the antennas, as well as the directive gain patterns in the x-z plane for both components of far-field. These results are shown in Figures 11 through 20 for the NMHD's near their first resonances, and in Figures 21 through 30 for the NMHD's near their second resonances. The phase plots in Figures 21, 25, 27, and 29 indicate an abrupt change in phase angle ϕ from -180° to $+180^\circ$. This 360° change has no physical significance and is due to the way ϕ is calculated, such that $-180^\circ \leq \phi \leq 180^\circ$.

It should be noted that the choice of the number of segments to use in approximating the NMHD is a compromise. In general, the use of more segments will result in more accuracy in the solution, but will require more computer time and storage area. A reasonable way to choose the number of segments to use, and that used here, involves a comparison of two solutions to the problem. First the problem should be solved using a small number of segments, perhaps six per turn. Then the same problem should be solved using a greater number of segments. By comparing these two solutions one can ascertain if the solution seems to have converged to the degree required. If not, then the use of more segments is necessary. Of particular usefulness in this comparison are plots of the current distribution. For the NMHD's considered here it was found that the calculated current distribution was somewhat irregular when one hundred fifty-one segments were used, while the distribution was smooth when two hundred fifty-one segments were used.

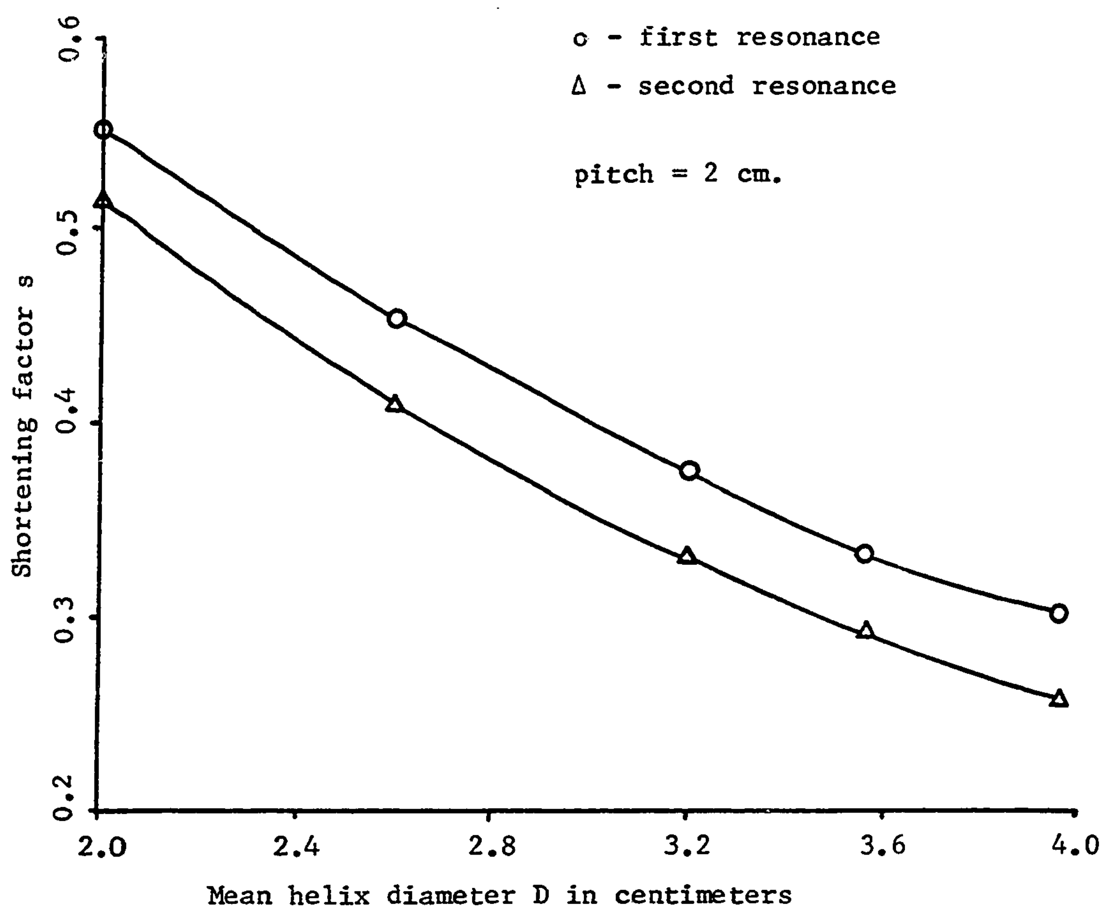

Figure 5. Shortening factor s as a function of mean helix diameter D

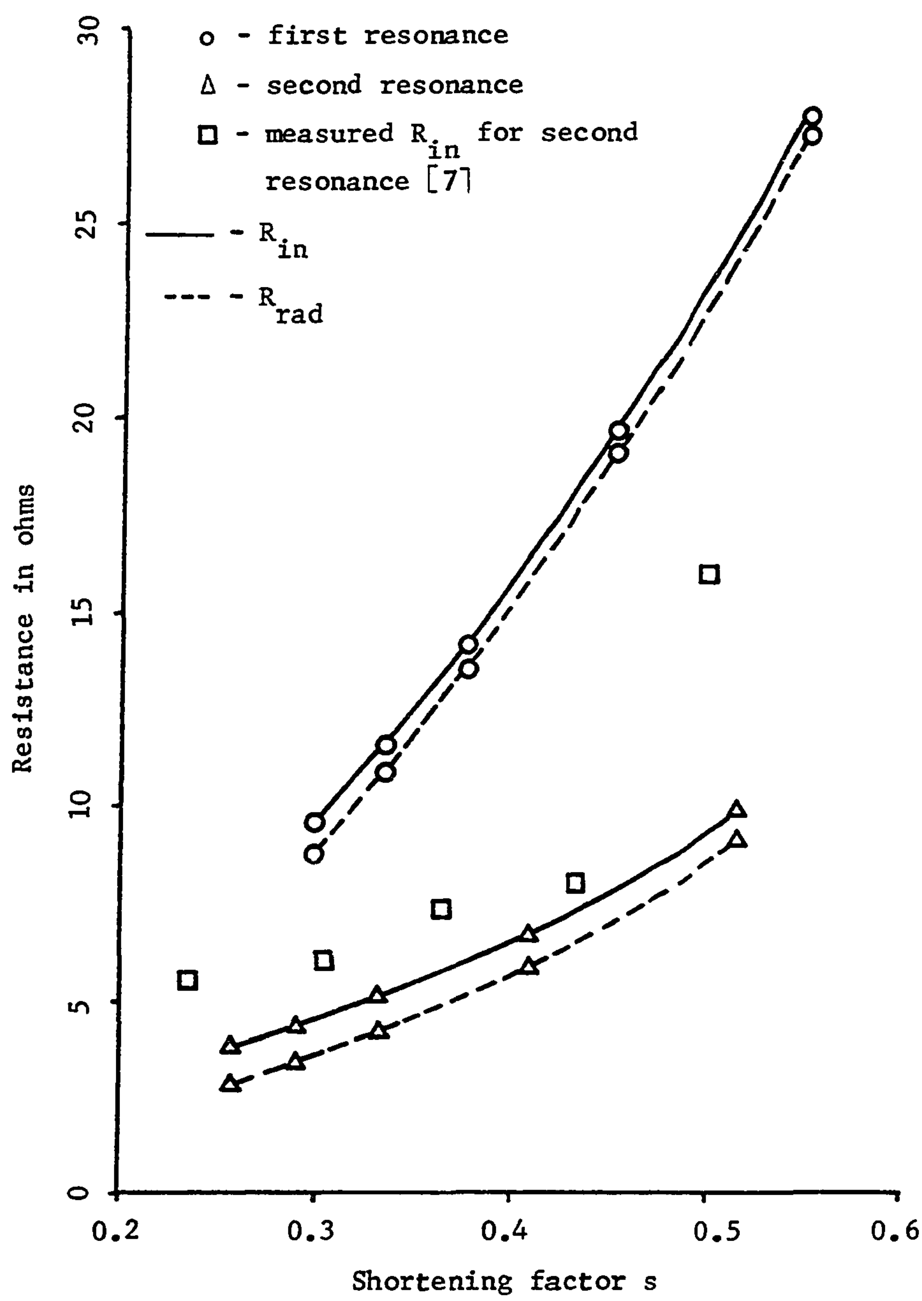

Figure 6. Input resistance R_{in} and radiation resistance R_{rad} as functions of shortening factor s

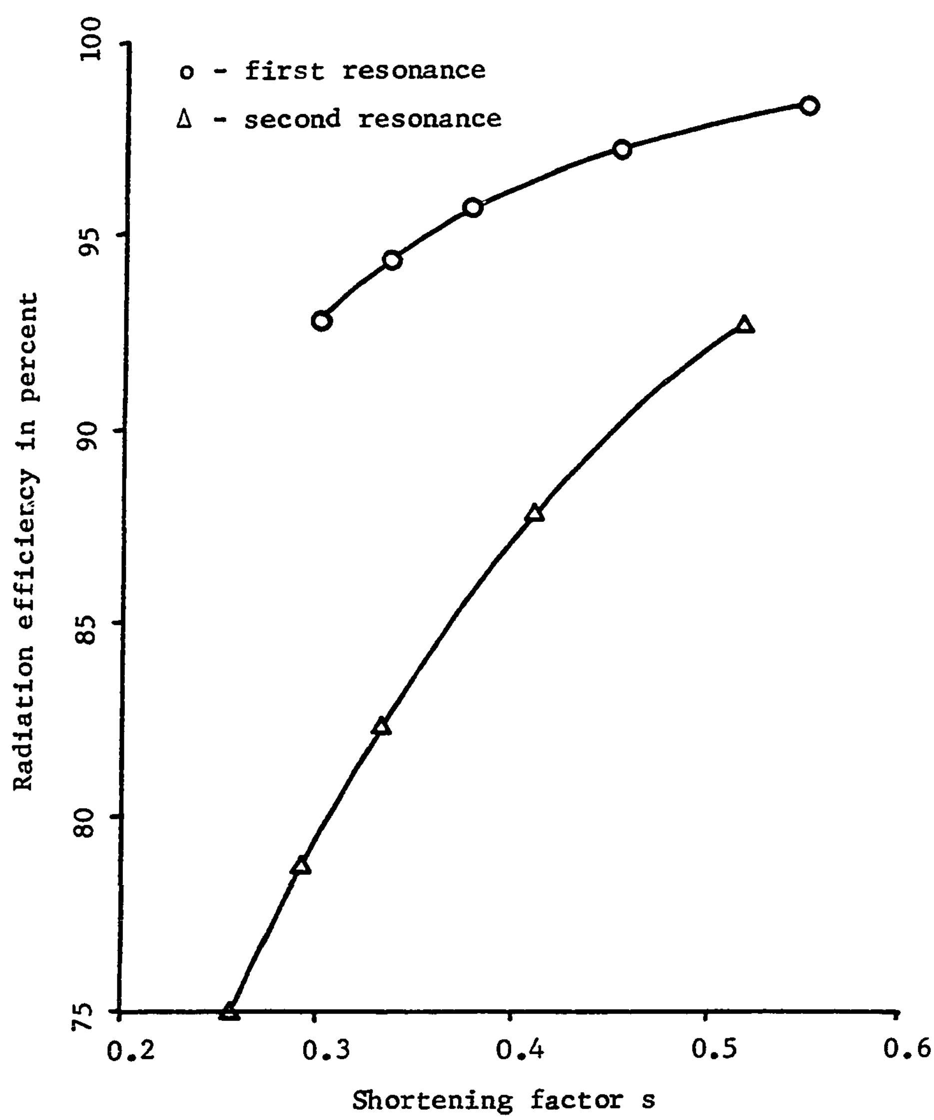

Figure 7. Radiation efficiency as a function of shortening factor s

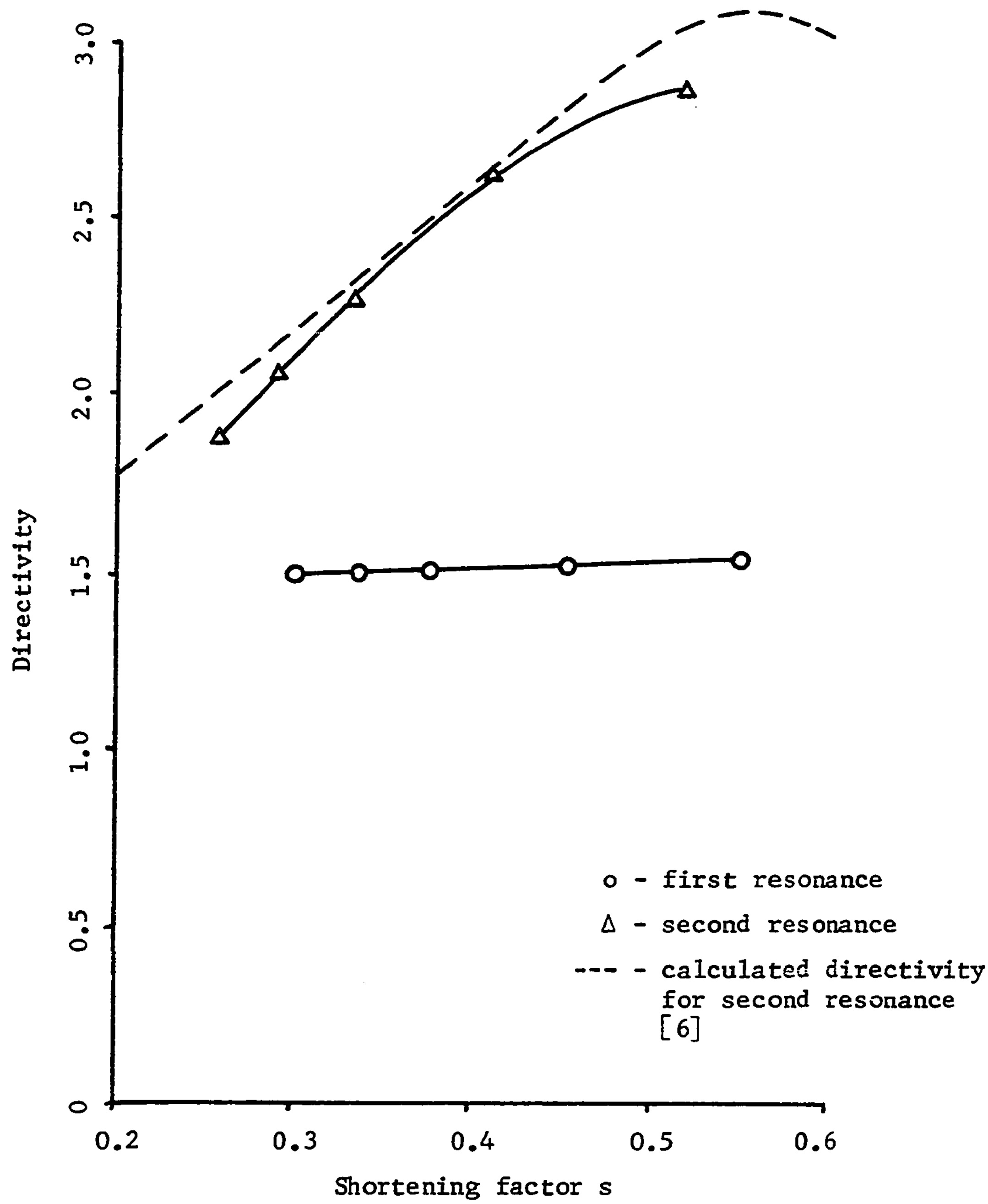

Figure 8. Directivity for θ-polarization as a function of shortening factor s

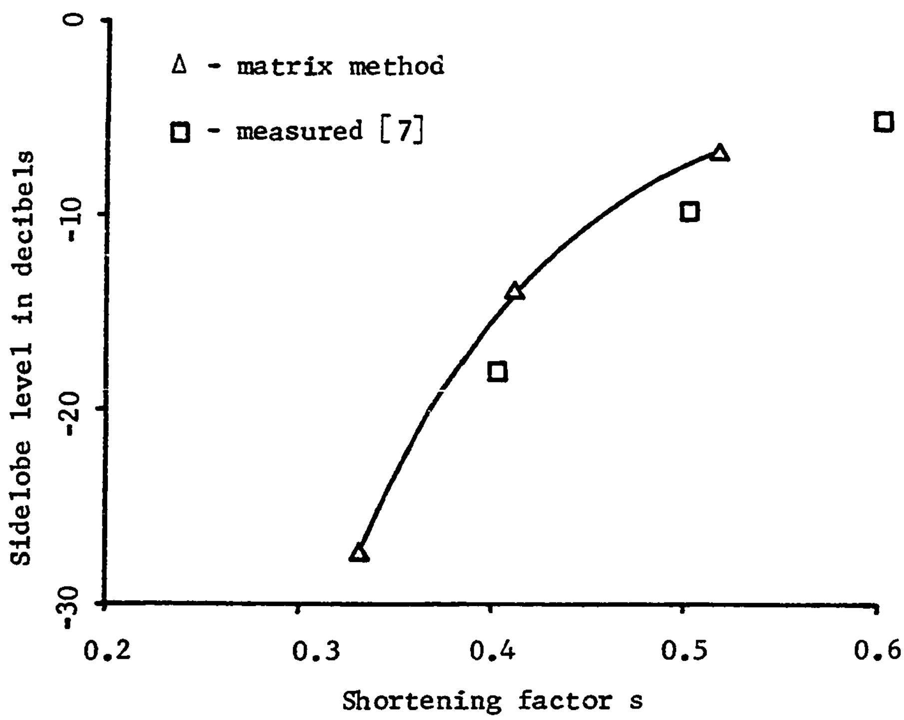

Figure 9. Sidelobe level as a function of shortening factor s at second resonance

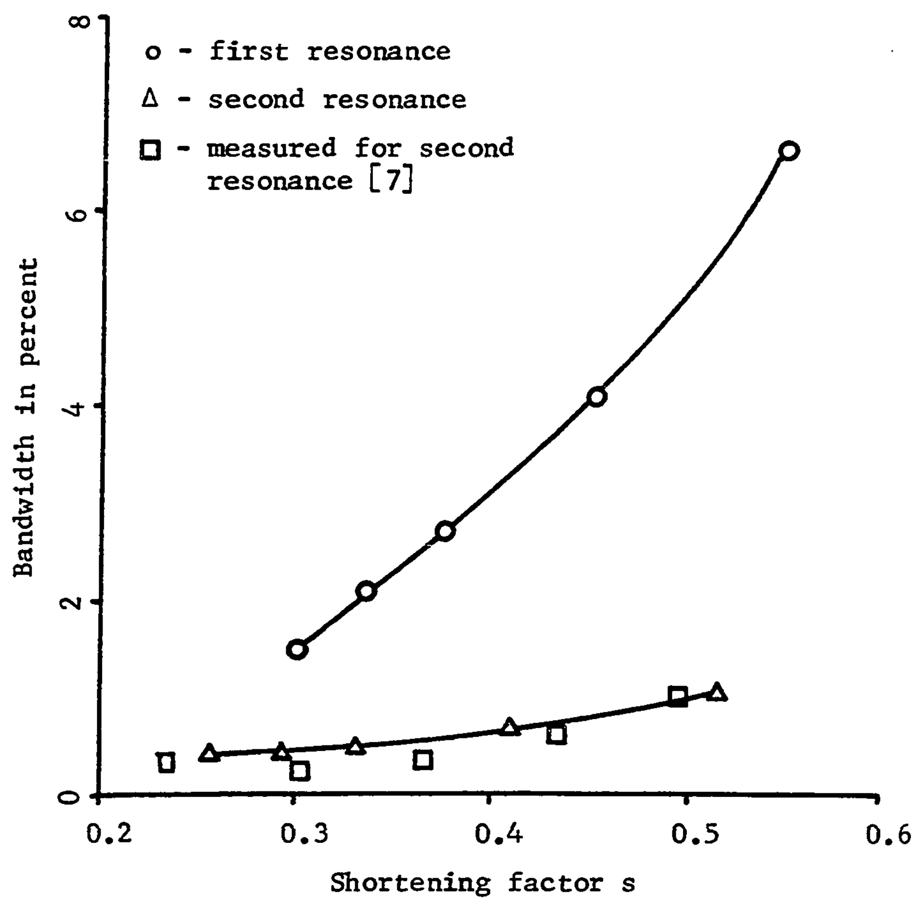

Figure 10. Bandwidth as a function of shortening factor s

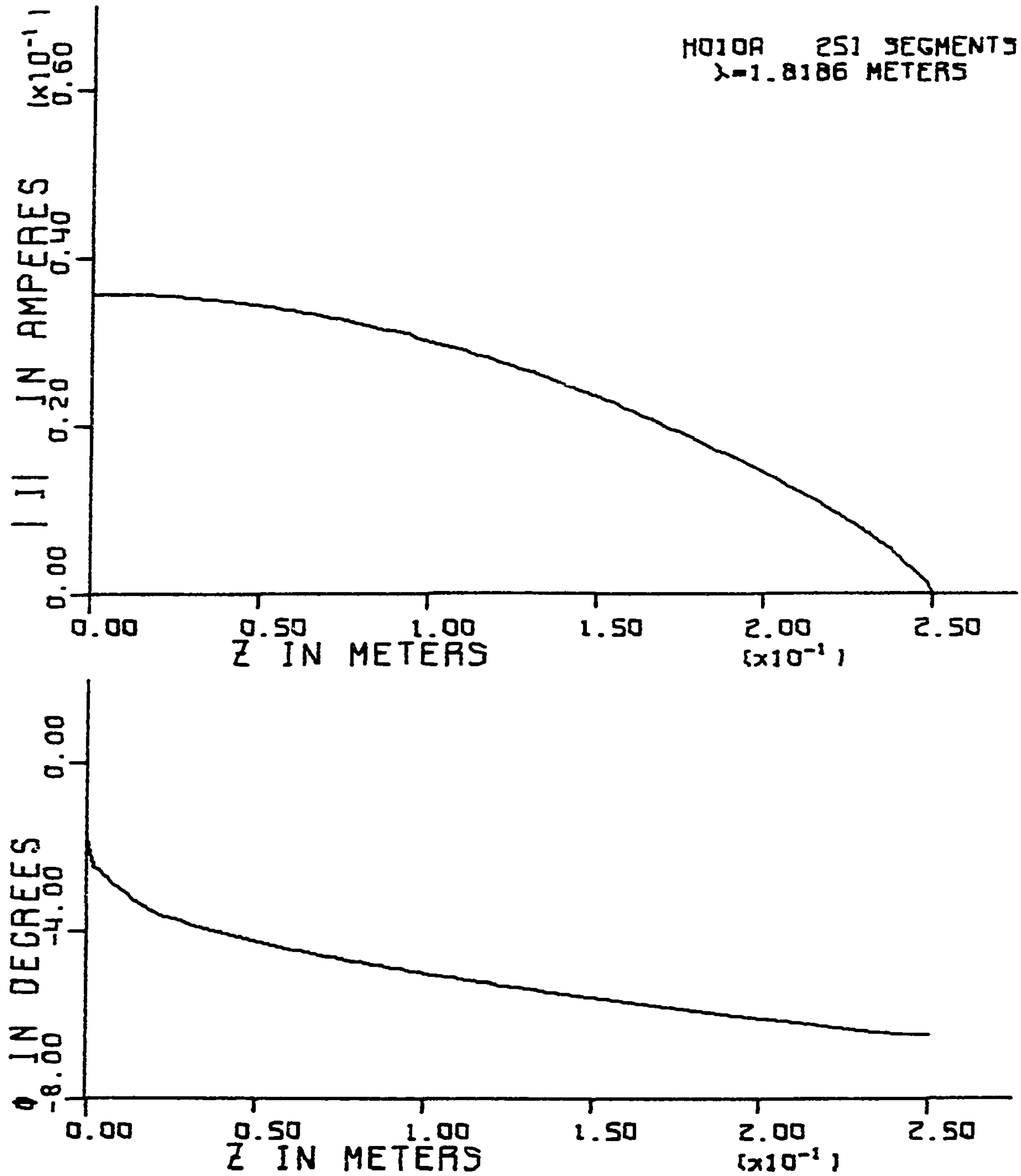

Figure 11. Current distribution for HD-10A near first resonance, 0.5493

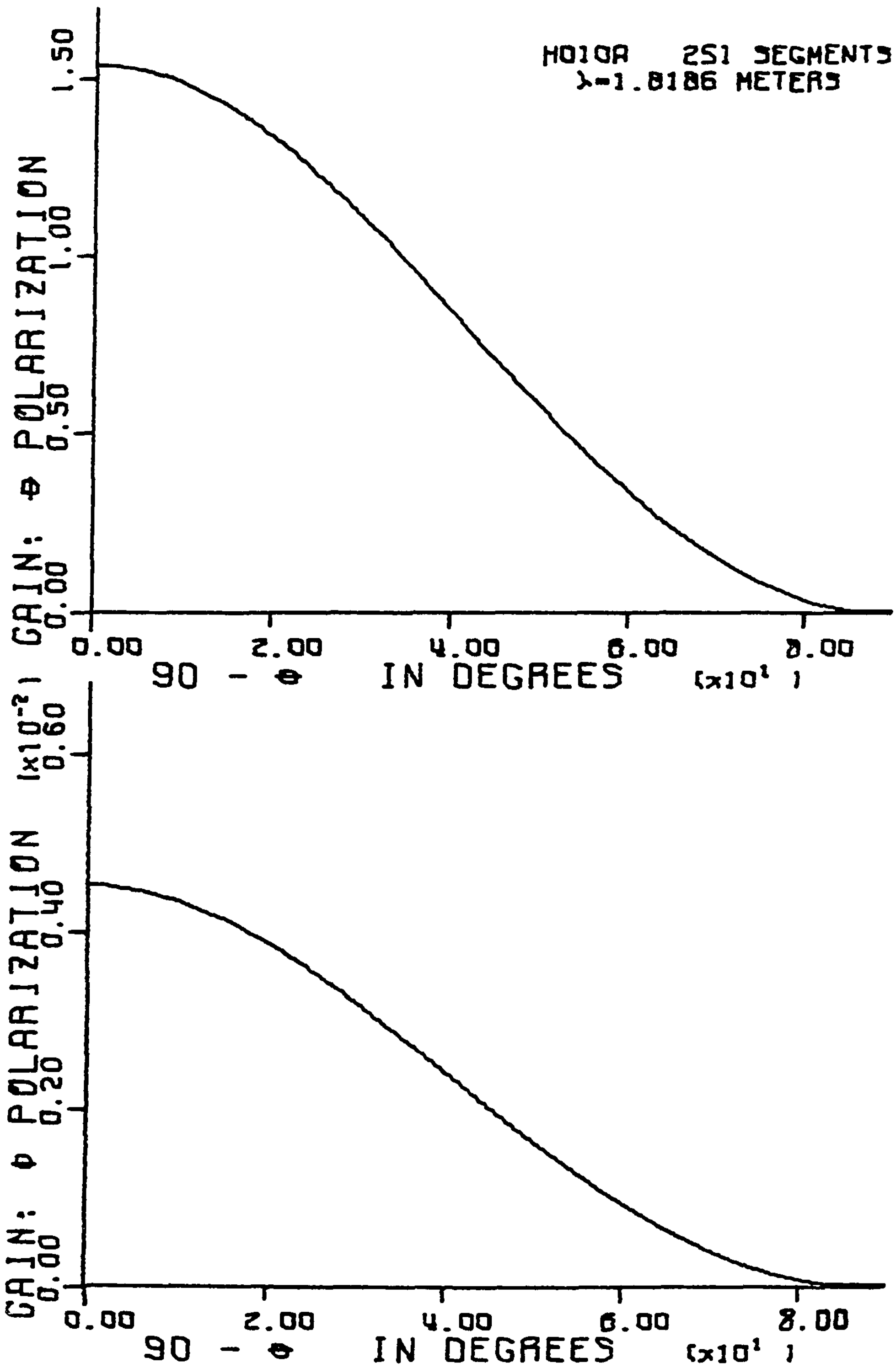

Figure 12. Directive gain for HD-10A near first resonance, s = 0.5493

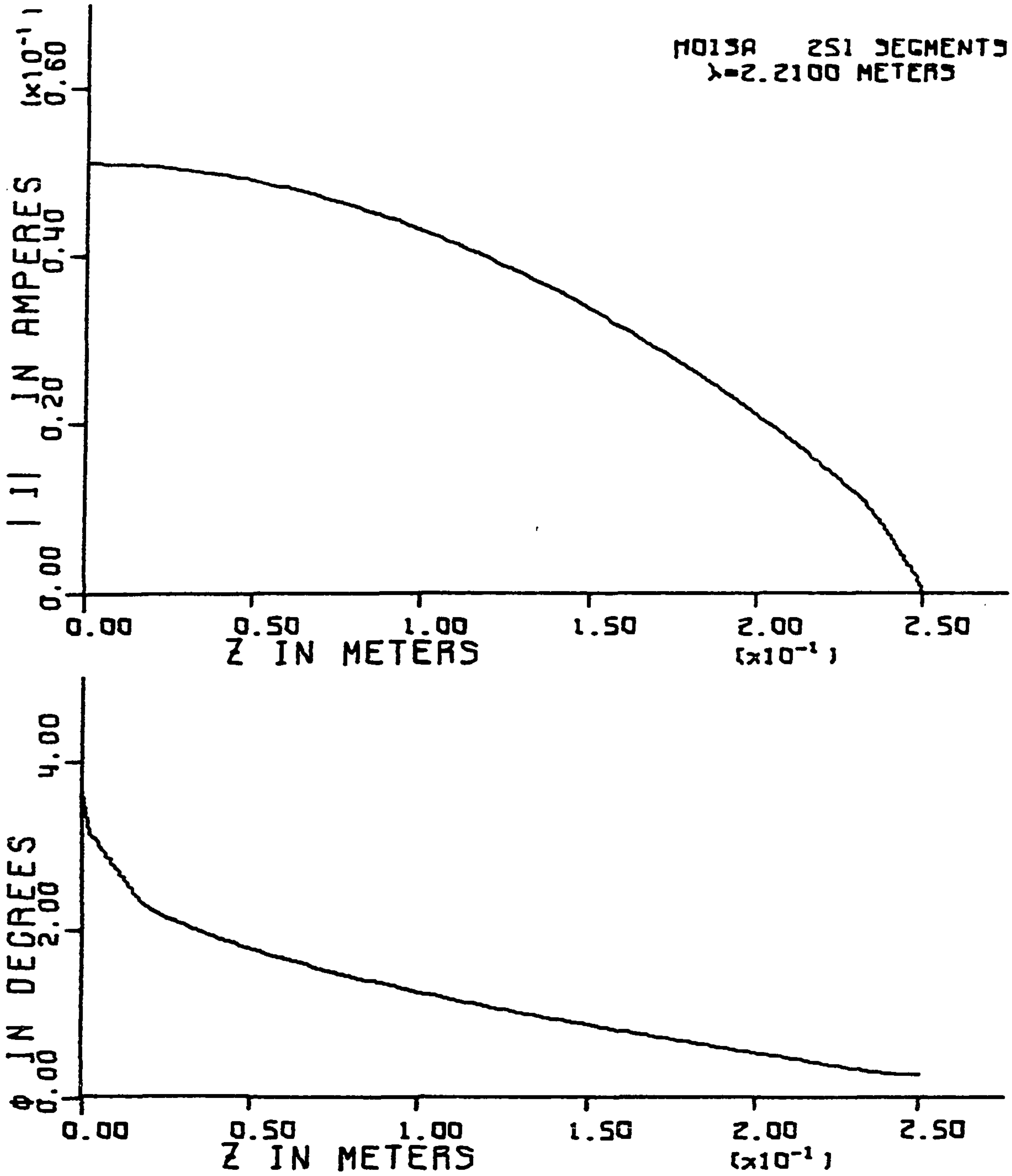

Figure 13. Current distribution for HD-13A near first resonance, s = 0.4531

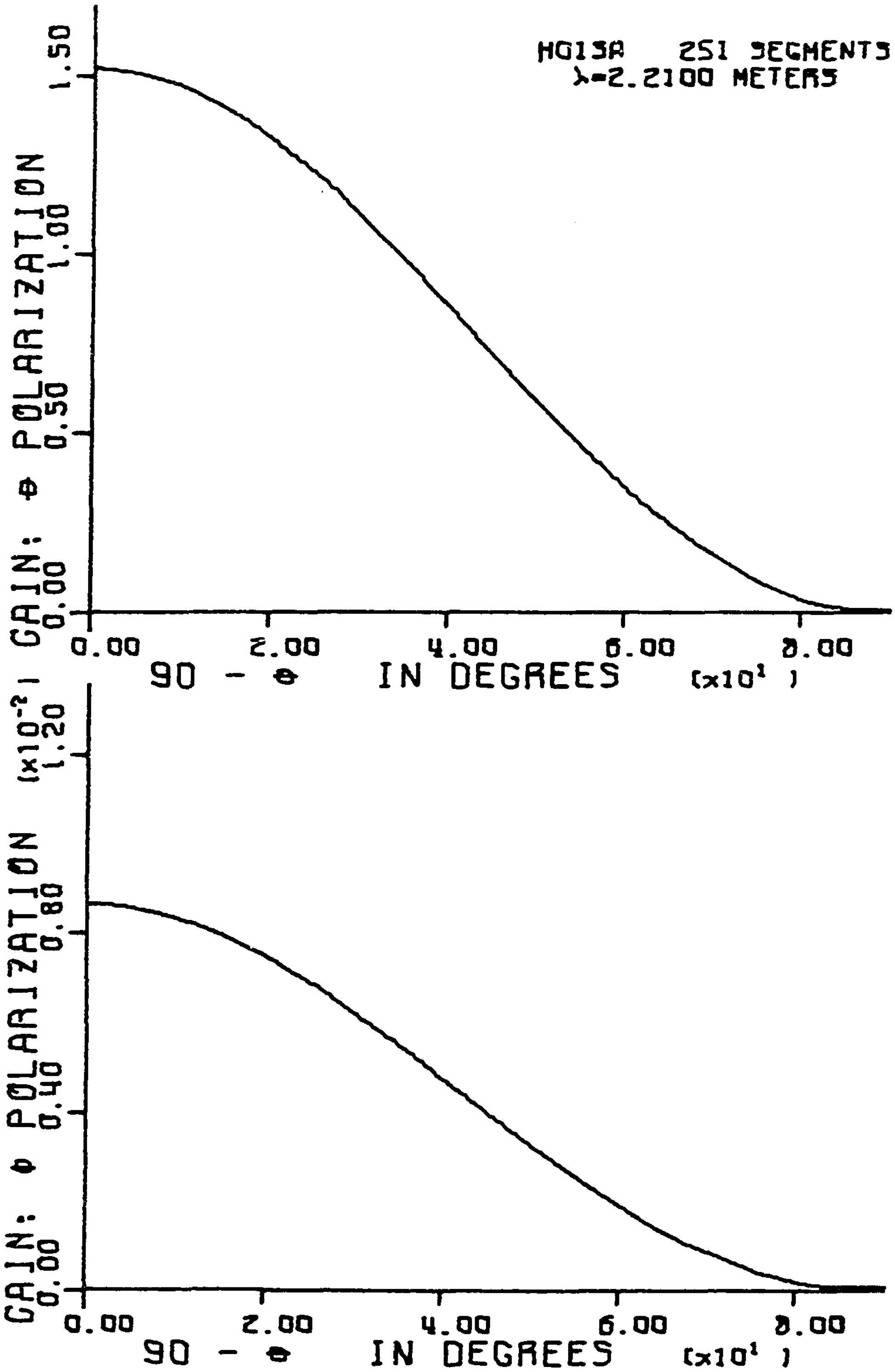

Figure 14. Directive gain for HD-13A near first resonance, s = 0.4531

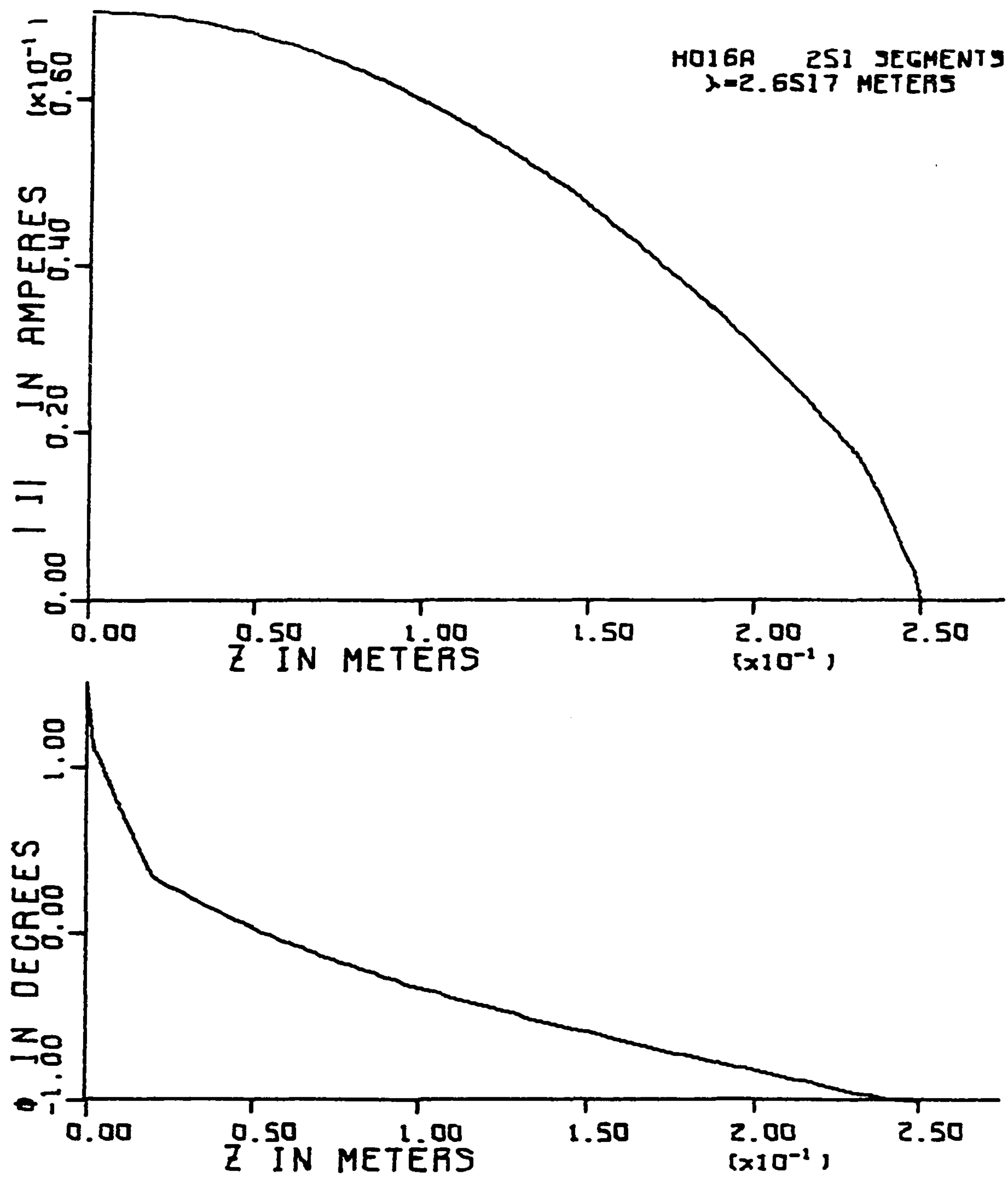

Figure 15. Current distribution for HD-16A near first resonance, s = 0.3772

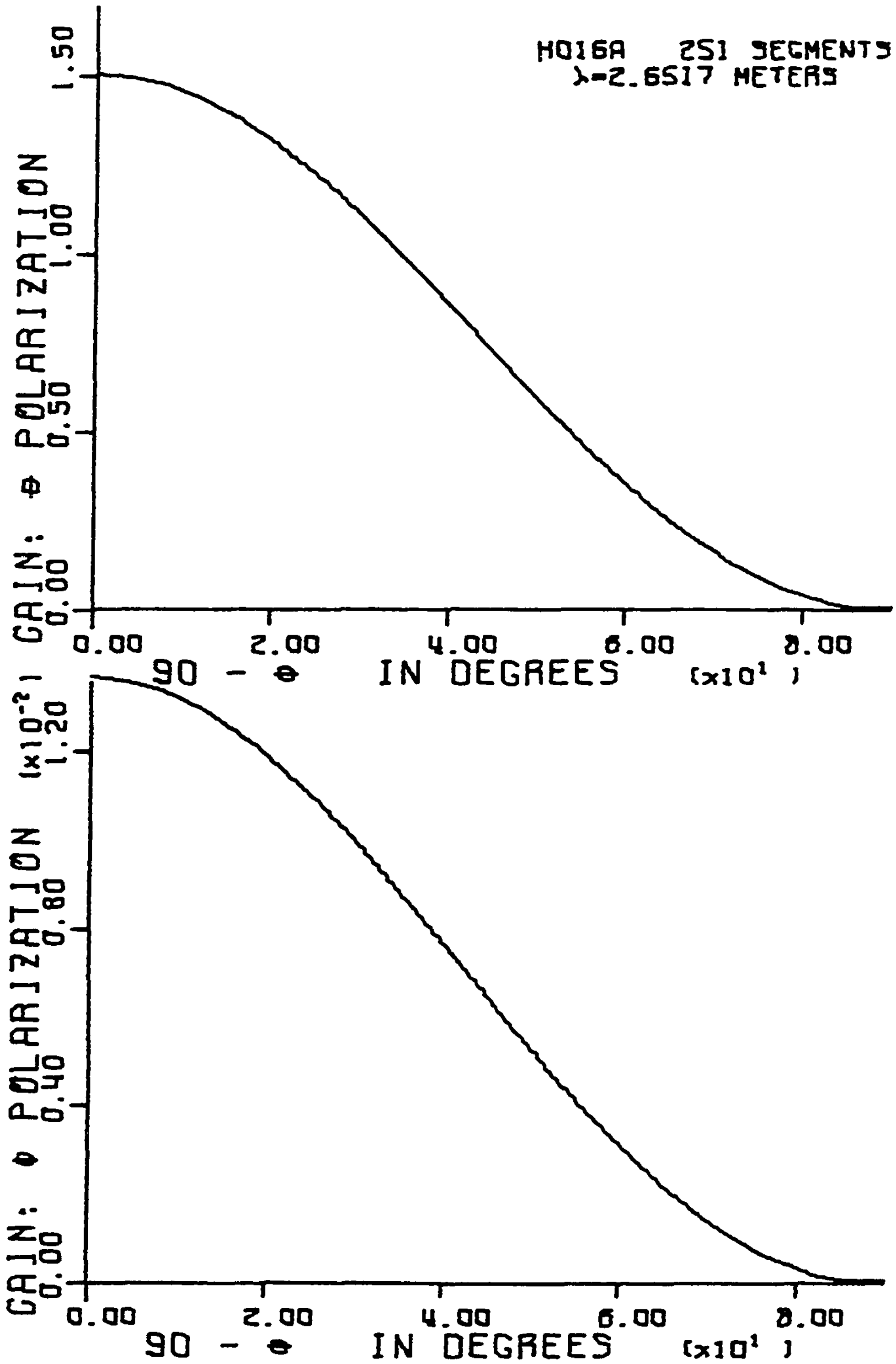

Figure 16. Directive gain for HD-16A near first resonance, s = 0.3772

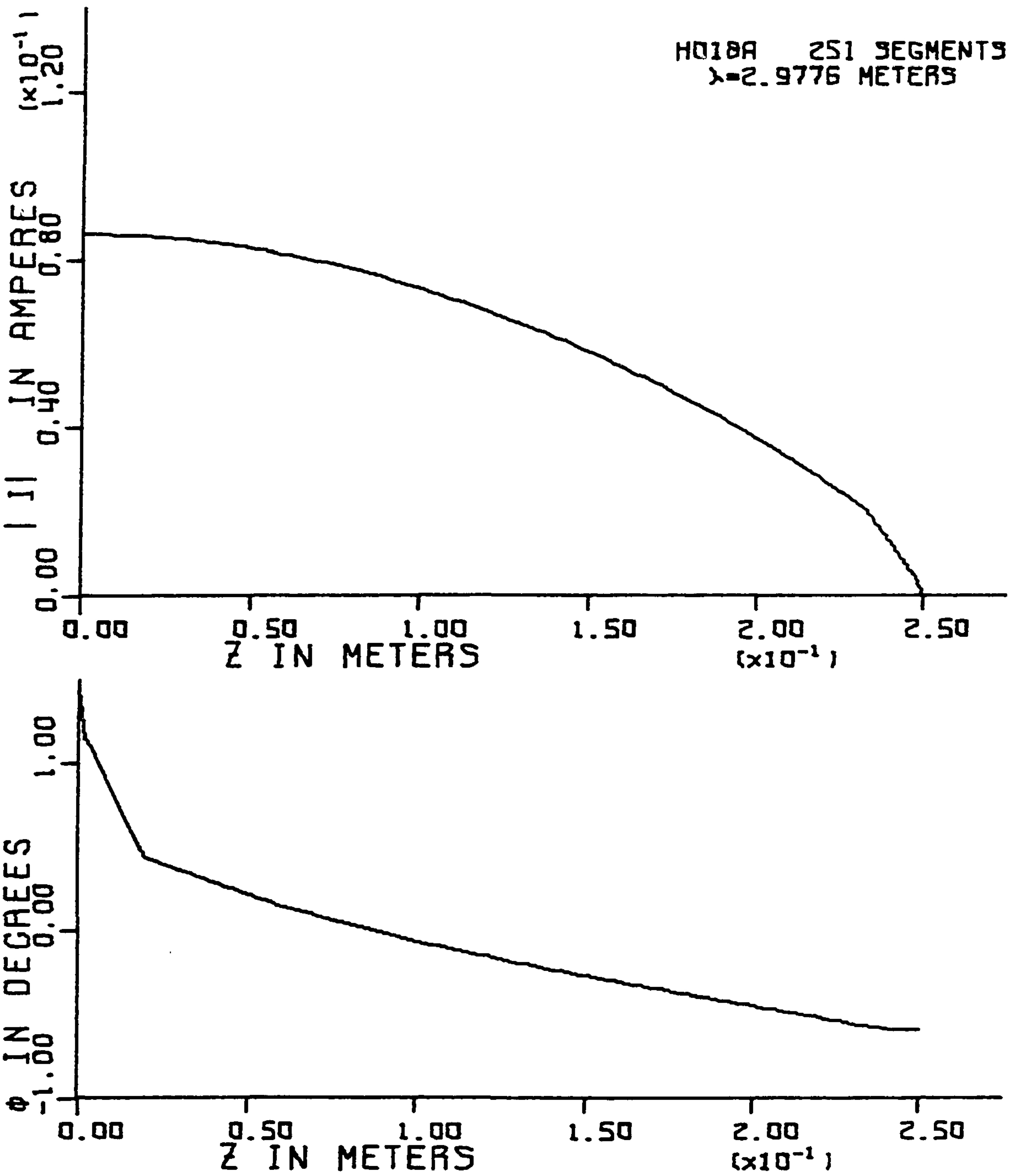

Figure 17. Current distribution for HD-18A near first resonance, 0.3359

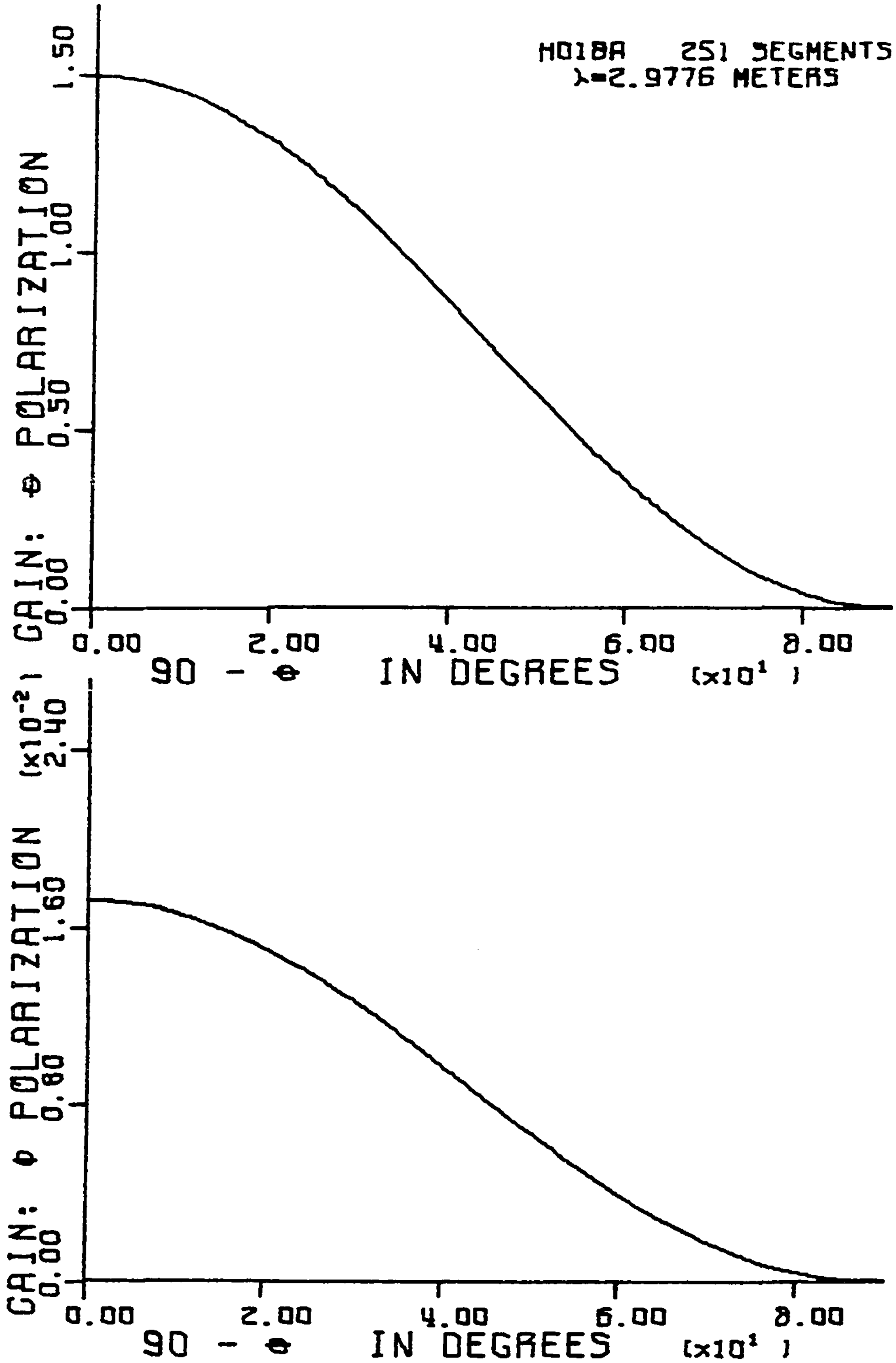

Figure 18. Directive gain for HD-18A near first resonance, s = 0.3359

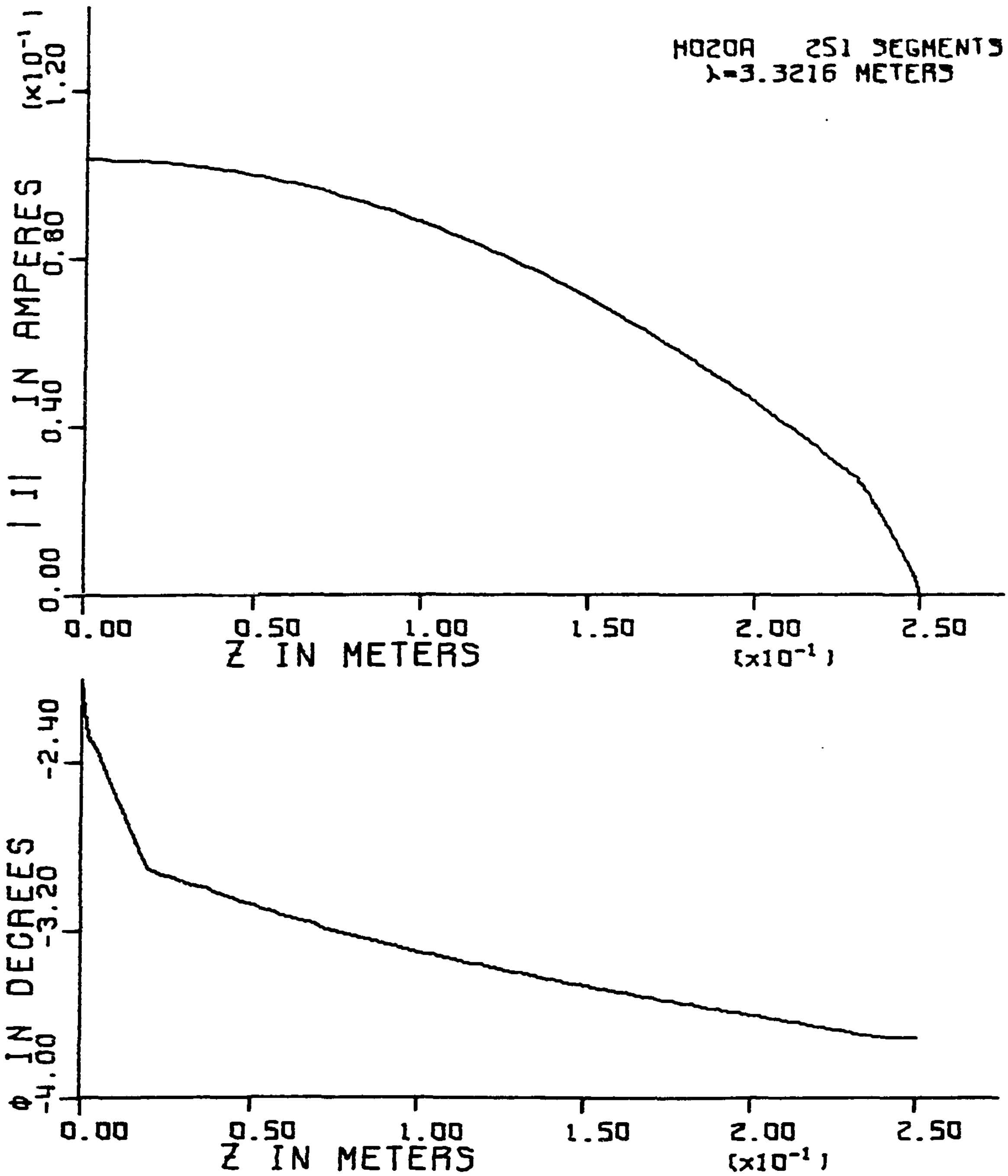

Figure 19. Current distribution for HD-20A near first resonance, 0.3010

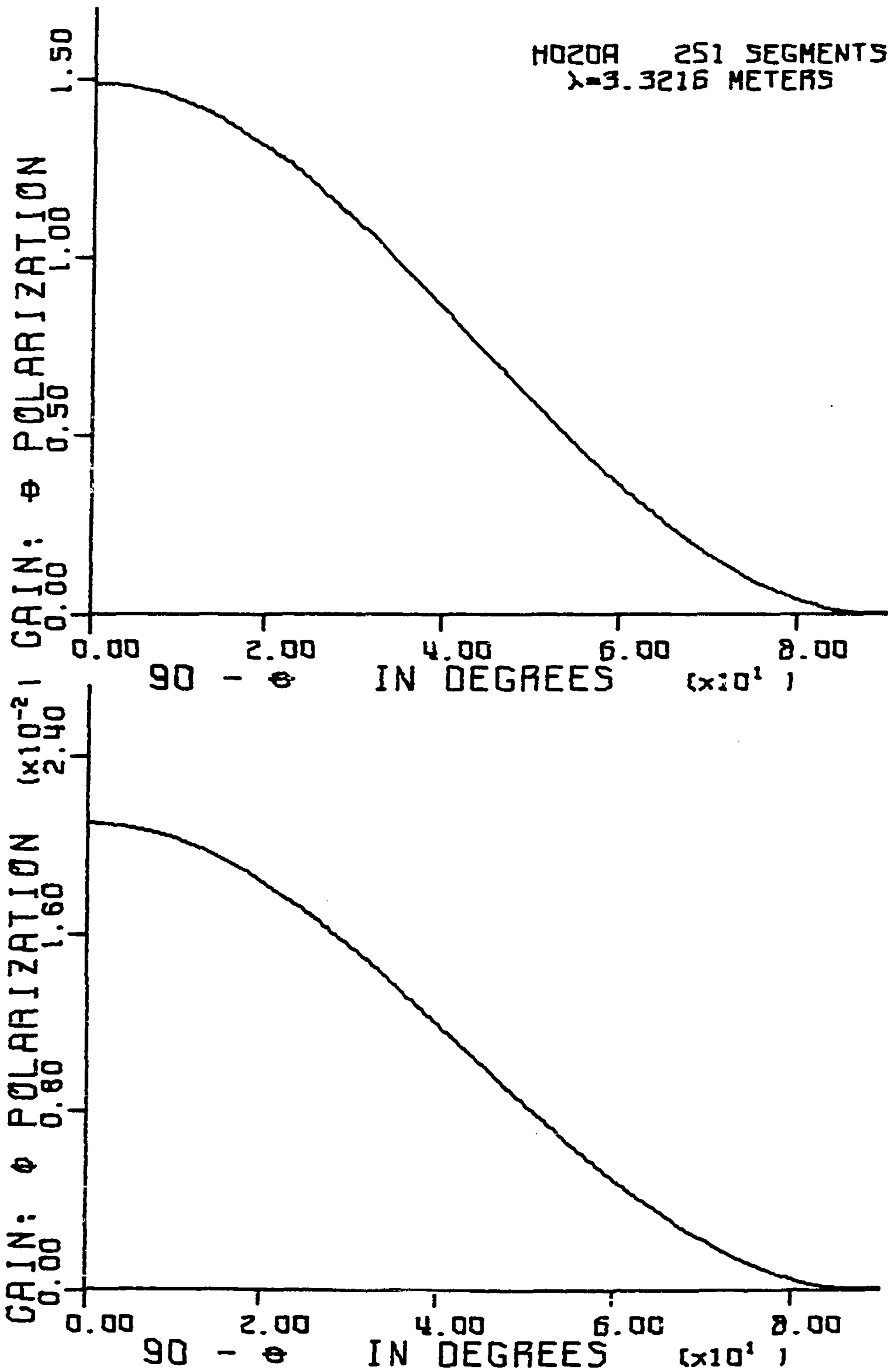

Figure 20. Directive gain for HD-20A near first resonance, s = 0.3010

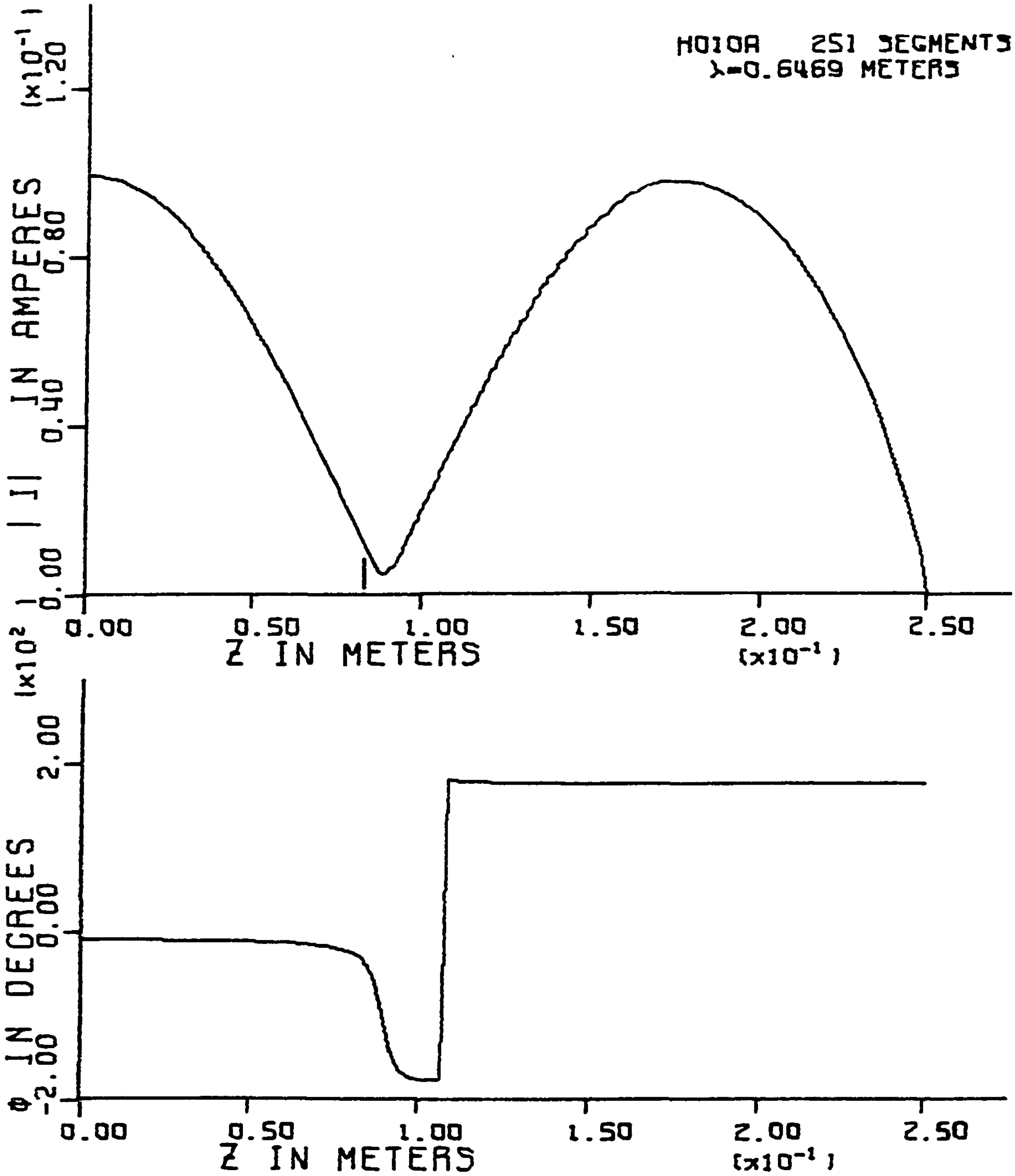

Figure 21. Current distribution for HD-10A near second resonance, s = 0.5150

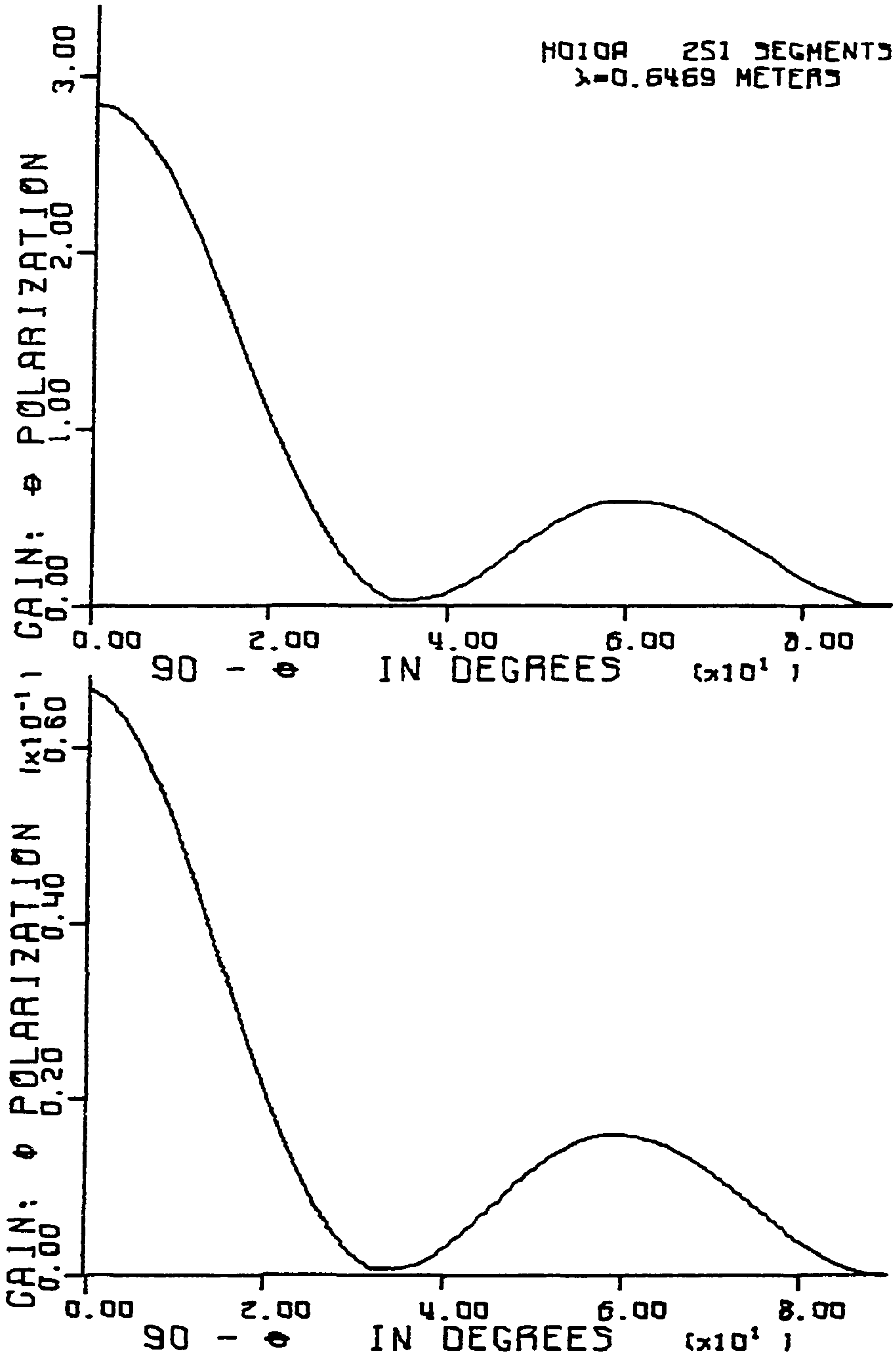

Figure 22. Directive gain for HD-10A near second resonance, s = 0.5150

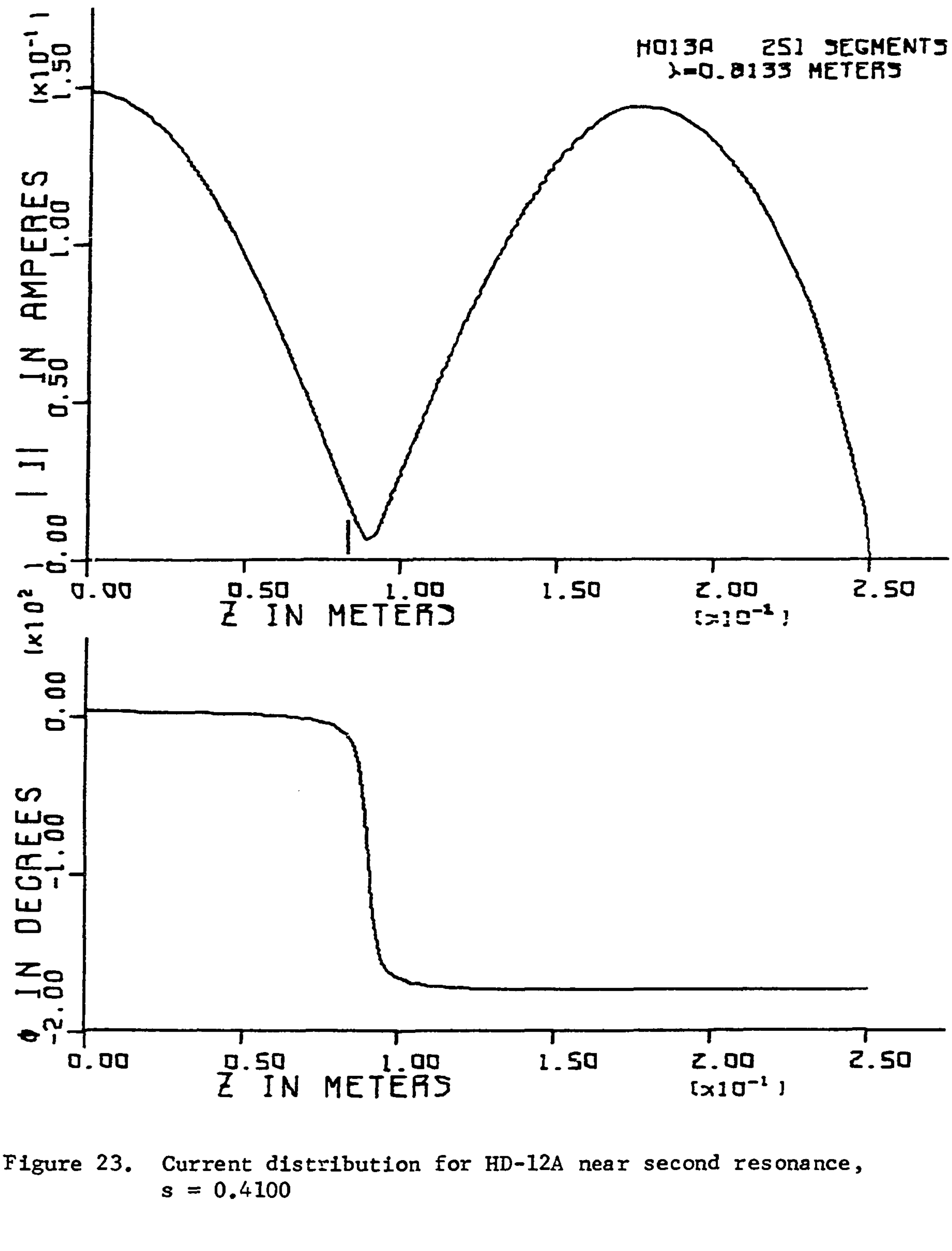

Figure 23. Current distribution for HD-12A near second resonance, s = 0.4100

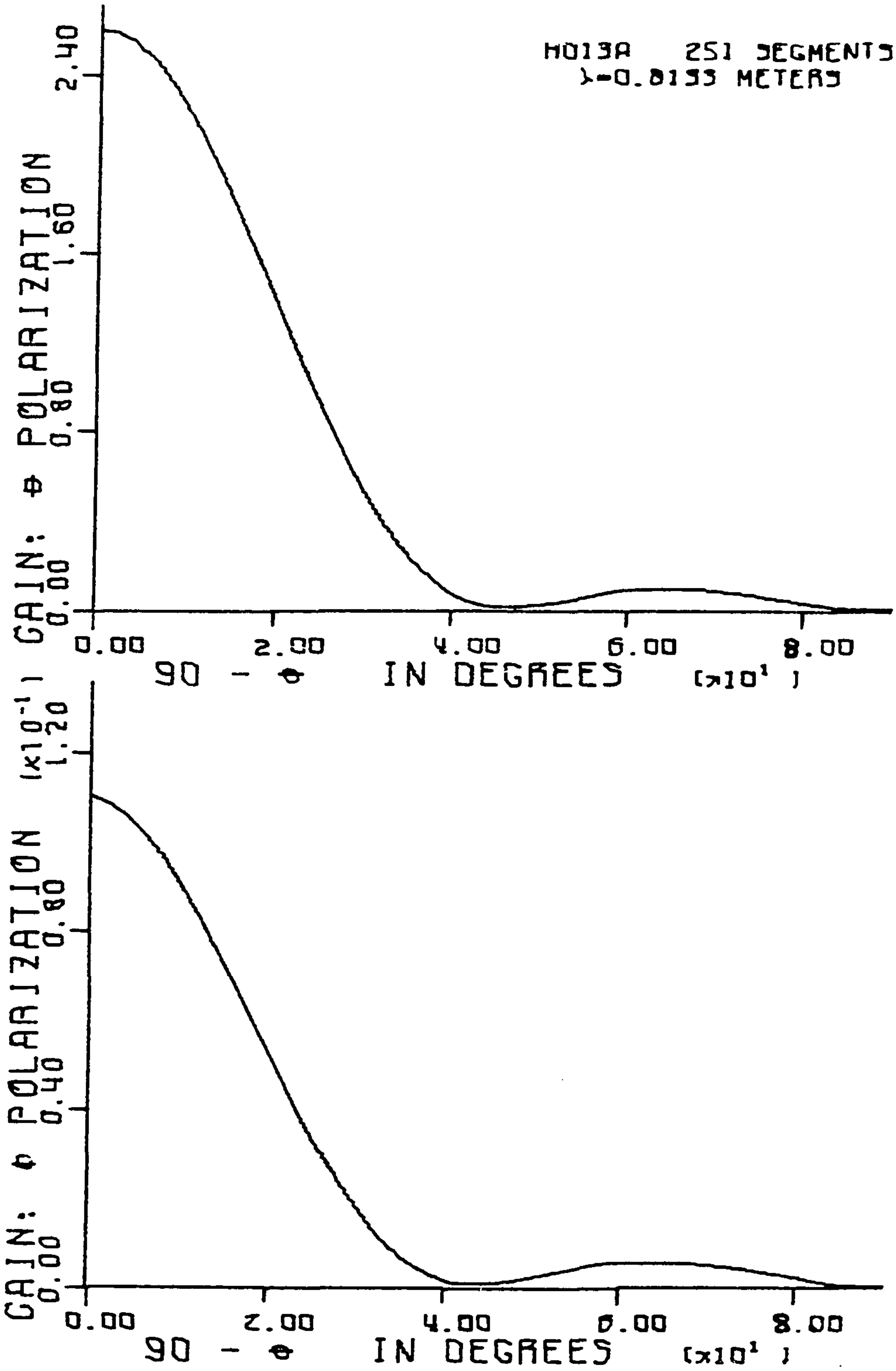

Figure 24. Directive gain for HD-13A near second resonance, s = 0.4100

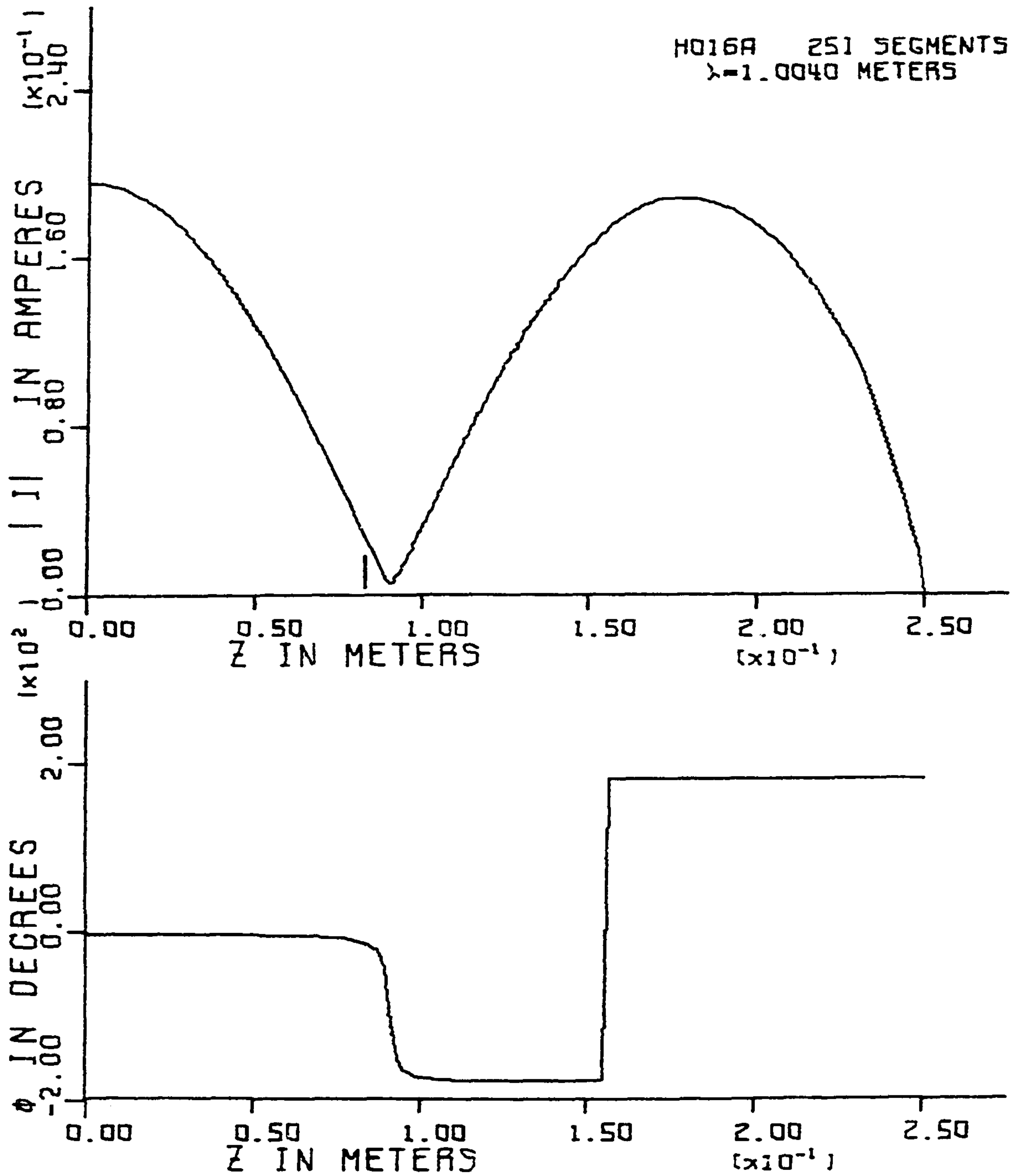

Figure 25. Current distribution for HD-16A near second resonance, s = 0.3320

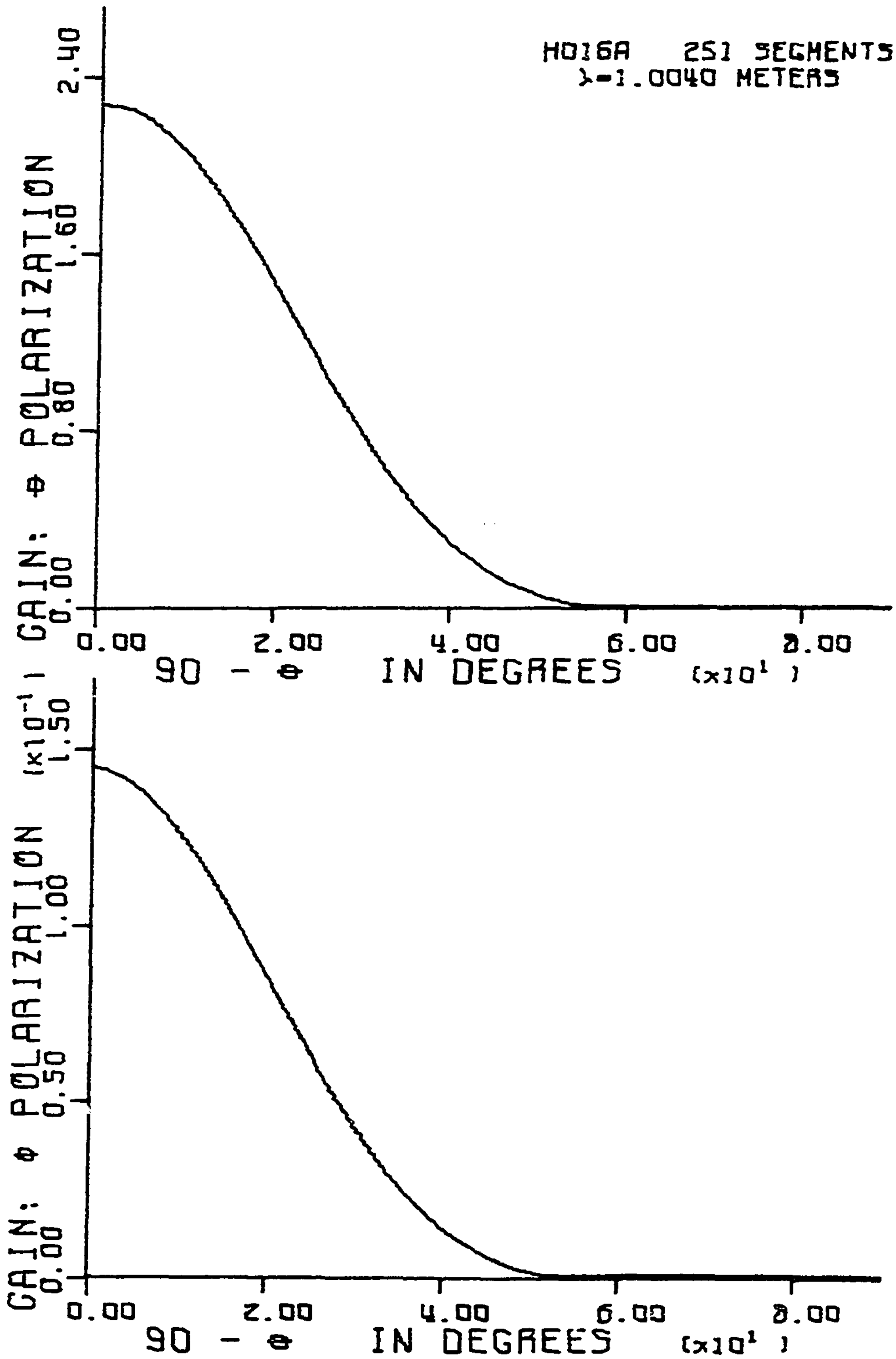

Figure 26. Directive gain for HD-16A near second resonance, s = 0.3320

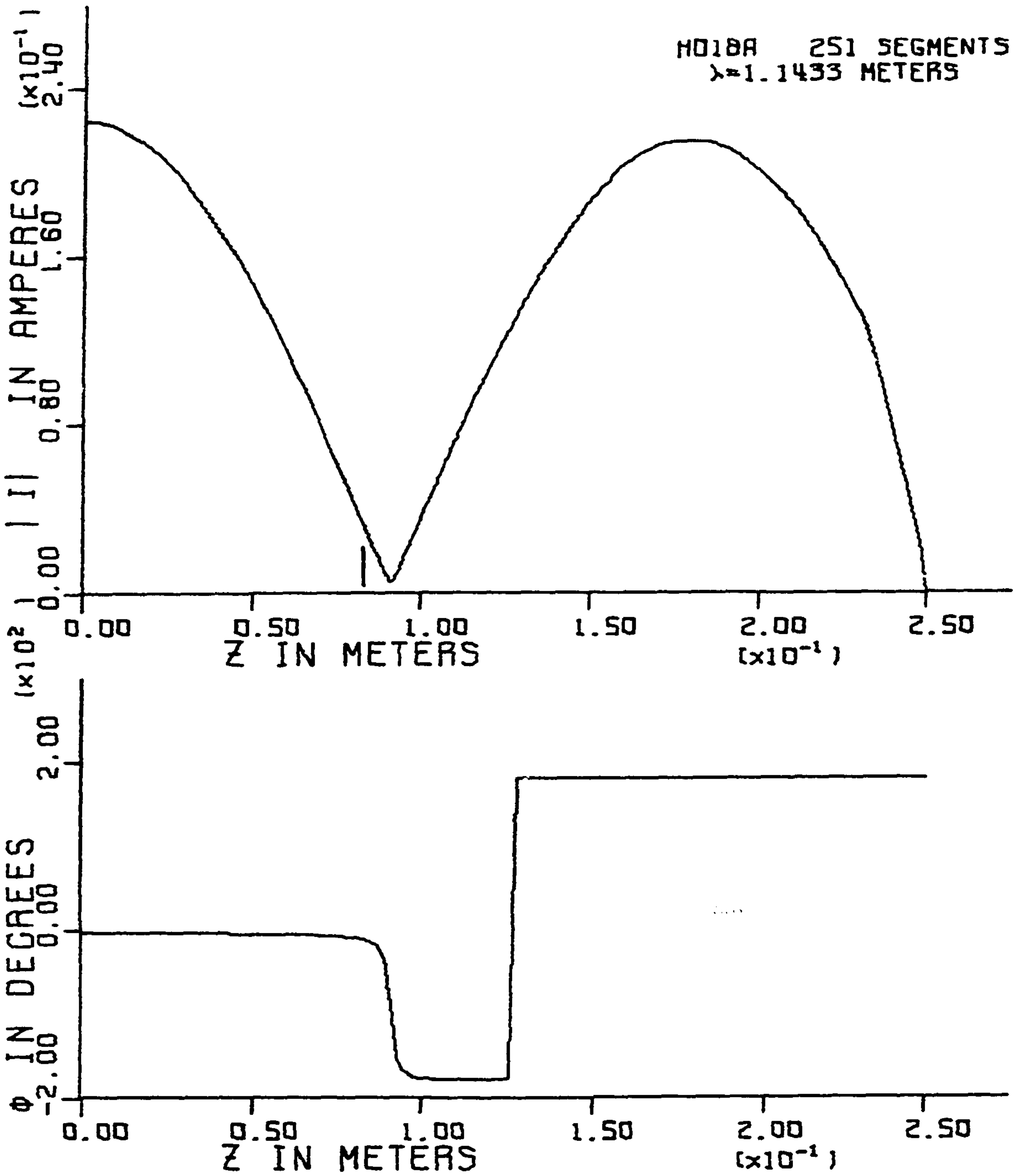

Figure 27. Current distribution for HD-18A near second resonance, s = 0.2915

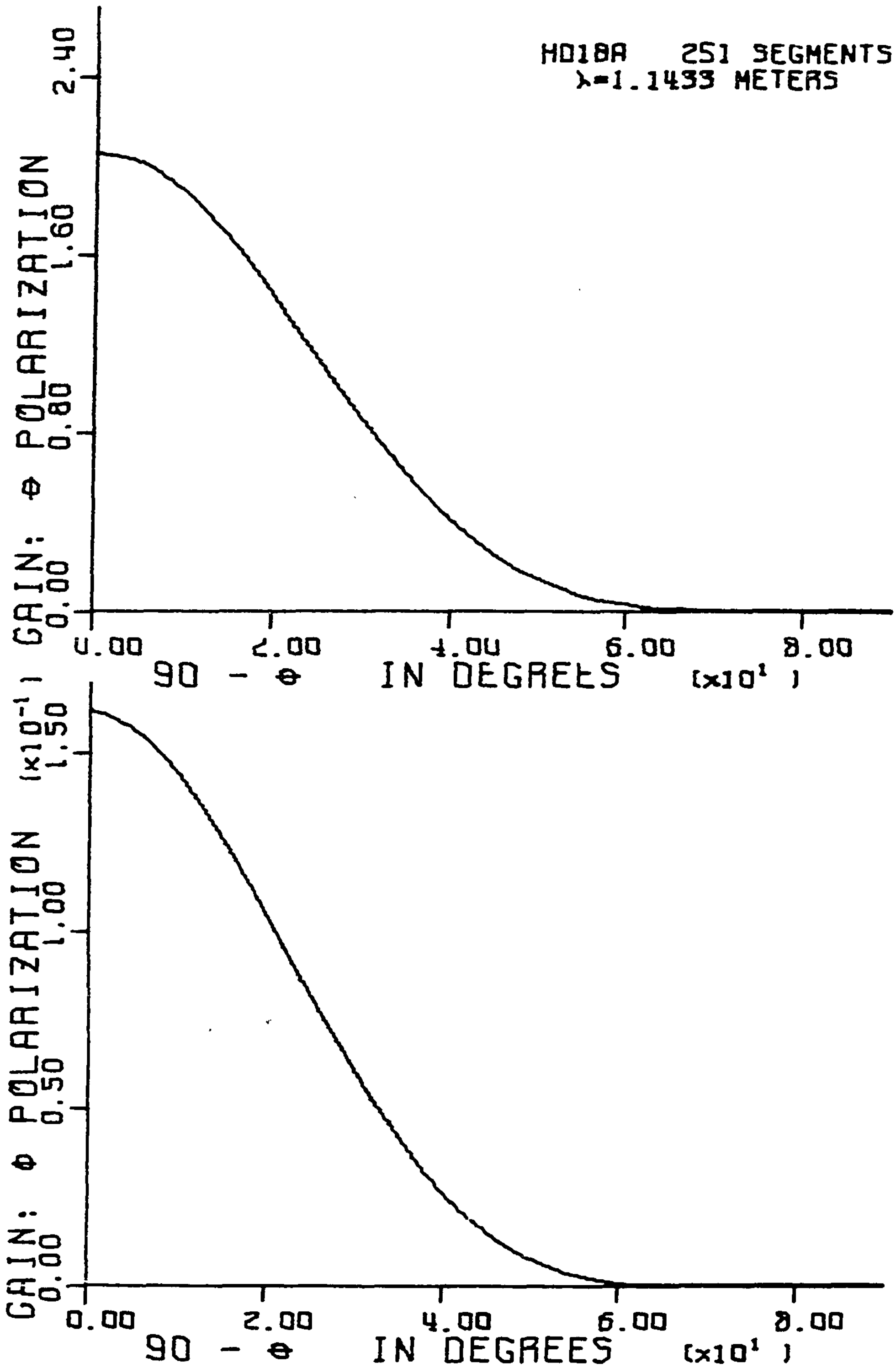

Figure 28. Directive gain for HD-18A near second resonance, s = 0.2915

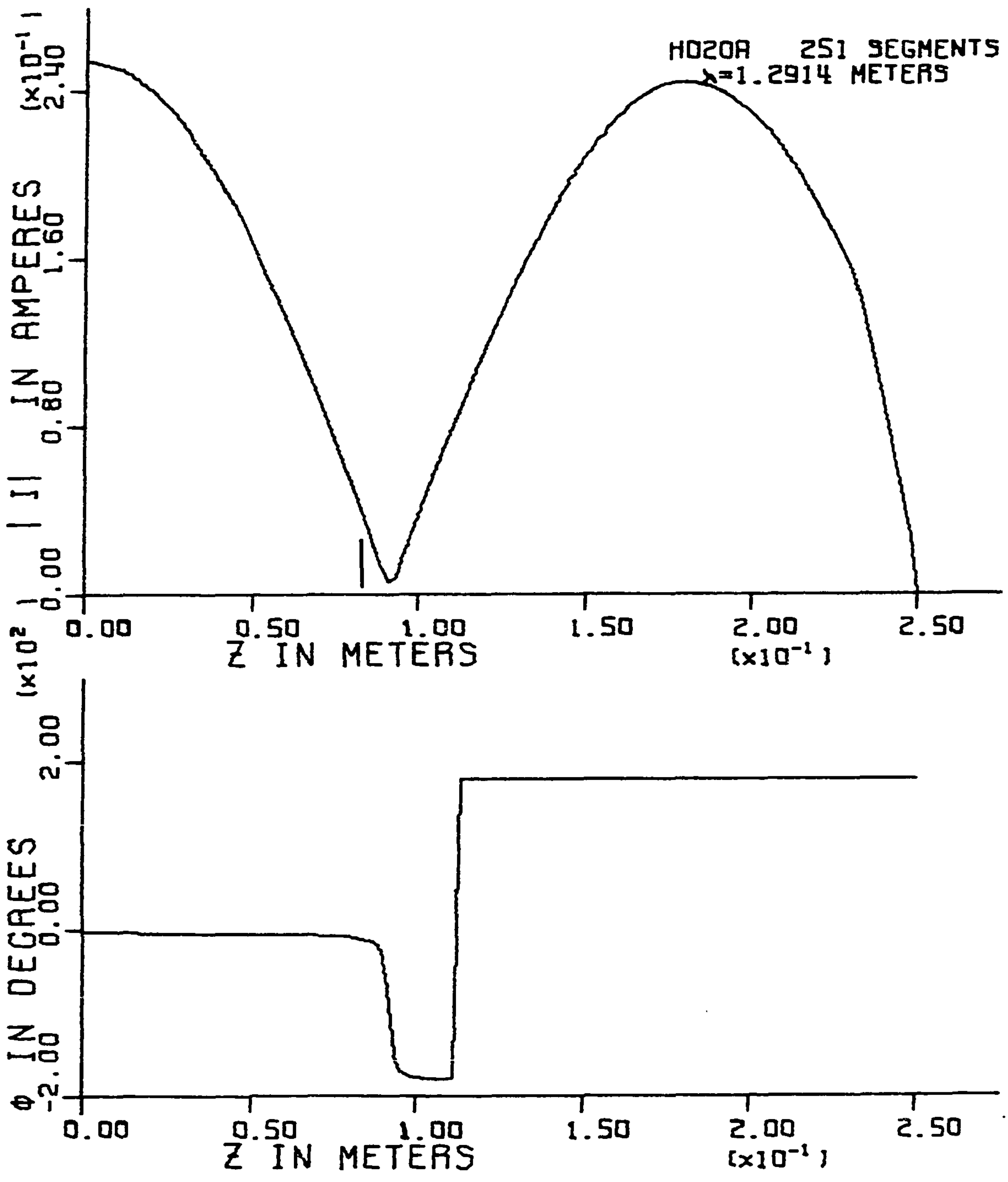

Figure 29. Current distribution for HD-20A near second resonance, s = 0.2581

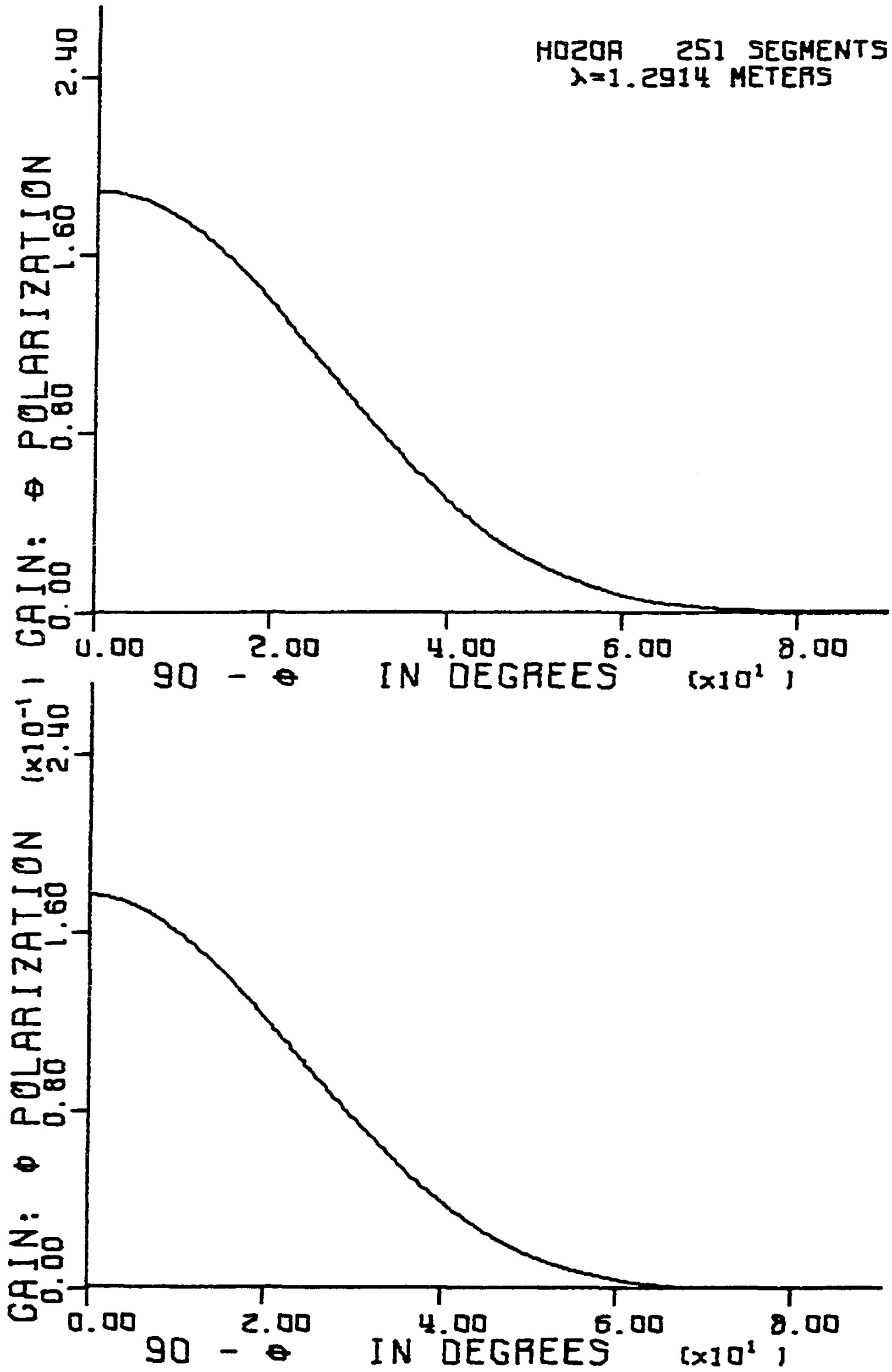

Figure 30. Directive gain for HD-20A near second resonance, s = 0.2581

V. DISCUSSION

While the number of numerical examples considered was small, the results do provide insight into the characteristics of the NMHD. Of particular interest are the calculated current distributions for the second resonance, shown in Figures 21, 23, 25, 27, and 29. If the current distribution were truly sinusoidal, then there would be a null in the current distribution at $z = h/3$. This value of z is indicated on the figures by a short vertical line. Note that the null actually occurs at a somewhat larger value of z. This null displacement indicates that the phase velocity for the finite helix is a function of position. This result has not, to the author's knowledge, been calculated previously. Note that the current distribution drops off rather abruptly near the end of the helix. This dropping off, or end effect, occurs along the last turn of the helix, and appears to be similar to the end capacitance effect for a linear dipole. The end effect indicates that the phase velocity is smaller near the helix end than near the midpoint. Also note that the peak in the current distribution at about $z = 0.17$ is not as big as the peak at $z = 0$. This suggests that the propagation constant is complex, a result not surprising in view of the lossy wire conductor considered here.

The radiation efficiency as a function of shortening factor is shown in Figure 7. Although the results shown are for only one size of copper wire, it is expected that the radiation efficiency for a NMHD would decrease as the diameter of the wire decreased. For example, when the wire size for HD-16A was reduced from number twelve to number eighteen in an additional numerical example, the calculated radiation efficiency for the second resonance changed from about eighty-two percent to about seventy percent.

As interesting comparison can be made between the second resonance input resistance calculated here and that measured by Lain, Ziolkowski, and Mayes [7]. As shown in Figure 6 the measured input resistance, for a given value of s, is greater than the calculated here. This apparent discrepancy is probably due to the fact that the geometry for the measured antennas was different than that for those considered here. Both the measured and the numerically modeled antennas were resonant in the same frequency range. The measured antennas consisted of A. W. G. number sixteen tinned copper wire for which the a.c. resistance per unit length at the resonant frequency is, depending on the tin thickness, about four times that for the number twelve copper wire considered here. Thus the losses for the measured antennas should be greater than those for the antennas considered here, and the input resistance for the measured antennas should be greater than for those considered here.

A comparison between the second resonance directivity determined here and the directivity that Stephenson and Mayes [6] calculated by assuming a sinusoidal current distribution is shown in Figure 8. The discrepancy for small values of s seems to be due to the fact that in the work of Stephenson and Mayes the diameter of the NMHD was assumed to be very small, so that the cross-polarized field was negligible. For the NMHD's considered here the cross-polarized field is not negligible, particularly for the small values of s. From Figure 30 where s = 0.2581, note that the directivity for the ϕ-polarization (the cross-polarization) is about 0.18, while that for the θ-polarization is about 1.89. When these are added the result is 2.07, which agrees well with Stephenson and Mayes' calculated value. In a similar manner the two curves can be made to agree closely for $s < 0.4$. The discrepancy for $s > 0.4$ is not well understood, but it is probably due to the fact that the current distribution on a NMHD is not quite sinusoidal.

The directivity for a linear half-wave dipole can be calculated to be 1.64 by assuming a sinusoidal current distribution. In one additional example the diameter of the helix was set to zero, such that the helix degenerated into a linear antenna. The directivity of this antenna was then calculated to be 1.64.

The ratio of the directivity for the θ-polarization to that for the ϕ-polarization is also of interest. The square root of this directivity ratio is equal to the axial ratio AR of the elliptically polarized field for the antenna. Kraus [1] develops a formula for axial ratio based on approximating a NMHD by a series of linear elements and loops. The formula is

$$AR = \frac{2p\lambda_o}{\pi^2 D^2} \tag{76}$$

When the axial ratio is calculated for HD-10A at its first resonance using (76), the result is 18.5. From Figure 21 the directivity ratio is found to be 339. The square root of this directivity ratio is 18.4, which compares very closely with that from Kraus' formula. In a similar manner the axial ratio determined from the results here for HD-20A in its first resonance is 8.41, compared to 8.44 using (76).

The sidelobe level calculated here for the second resonance is compared to that measured by Lain, Ziolkowski, and Mayes [7] in Figure 9. The agreement is pretty close, allowing for the somewhat different antenna geometries. In both the calculations and the measurements the sidelobe structure was found to disappear for s less than about 0.3.

Second resonance bandwidths calculated here and those measured by Lain, Ziolkowski, and Mayes [7] are compared in Figure 10. Again the agreement is probably as close as can be expected, considering the differing geometries.

In conclusion, the matrix method has been used to solve the NMHD problem, and has yielded results comparable to those obtained by other investigators. Of particular significance here are the results which indicate that the phase velocity along the finite helix is a function of position. This conclusion cannot be reached on the basis of the sinusoidal current distribution assumed by others, and would be quite difficult to measure.

The computer program listed in the Appendix can be used for additional numerical investigations of the NMHD. The user is cautioned to consider his problem carefully before applying this program to an arbitrary NMHD. In particular, he should ascertain that the assumptions upon which this method is based are satisfied for his problem.

VI. REFERENCES

[1] J. D. Kraus, Antennas. New York: McGraw-Hill, 1950.

[2] J. D. Kraus, Radio Astronomy. New York: McGraw-Hill, 1966.

[3] R. E. Collin and F. J. Zucker, Antenna Theory, part 2. New York: McGraw-Hill, 1969, sect. 19.12.

[4] D. T. Stephenson, "Broadband helical dipole arrays," Antenna Laboratory Report No. 65-19, Engineering Experiment Station, University of Illinois, Urbana, October 1965.

[5] H. A. Wheeler, "A helical antenna for circular polarization," Proc. IRE, vol. 35, pp. 1484-1488, December 1947.

[6] D. T. Stephenson and P. E. Mayes, "Normal-mode helices as moderately superdirective antennas," IEEE Trans. Antennas Propagat., vol. AP-14, pp. 108-110, January 1966.

[7] W. Y. Lain, F. P. Ziolkowski, and P. E. Mayes, "The characteristics of normal mode helical dipoles near higher order resonances," Antenna Laboratory Report No. 66-7, Engineering Experiment Station, University of Illinois, Urbana, June 1966.

[8] T. Li, "The small-diameter helical antenna and its input characteristics," Ph.D. thesis, Dep. Elec. Eng., Northwestern University, Evanston, 1958.

[9] S. Sensiper, "Electromagnetic wave propagation on helical structures," Proc. IRE, vol. 43, pp. 149-161, February 1955.

[10] P. W. Klock, "A study of wave propagation of helices," Antenna Laboratory Report No. 68, Engineering Experiment Station, University of Illinois, Urbana, March 1963.

[11] J. A. Marsh, "Current distributions on helical antennas," Proc. IRE, vol. 39, pp. 668-675, June 1951.

[12] R. W. P. King, The Theory of Linear Antennas. Cambridge: Harvard University Press, 1956.

[13] R. F. Harrington, "Matrix methods for field problems," Proc. IEEE, vol. 55, pp. 136-149, February 1967.

[14] R. F. Harrington, Field Computation by Moment Methods. New York: Macmillan, 1968.

[15] R. F. Harrington and J. R. Mautz, "Straight wires with arbitrary excitation and loading," IEEE Trans. Antennas Propagat., vol. AP-15, pp. 502-515, July 1967.

[16] B. J. Strait and K. Hirasawa, "Computer programs for analysis and design of linear arrays of loaded wire antennas," Scientific Report No. 5 on Contract No. F19628-68-C-0180, AFCRL-70-0108, Syracuse University, February 1970.

[17] H. H. Chao and B. J. Strait, "Computer programs for radiation and scattering by arbitrary configurations of bent wires," Scientific Report No. 7 on Contract No. F19628-68-C-0180, AFCRL-70-0374, Syracuse University, September 1970.

[18] L. Fox, An Introduction to Numerical Linear Algebra. New York: Oxford University Press, 1965.

[19] J. H. Wilkinson, The Algebraic Eigenvalue Problem. Oxford: Clarendon Press, 1965.

[20] IBM System/360: FORTRAN IV Library Subprograms, Form C28-6596-2, 1966.

[21] W. L. Weeks, Antenna Engineering. New York: McGraw-Hill, 1968.

[22] E. C. Jordan and K. G. Balmain, Electromagnetic Waves and Radiating Systems, second edition. Englewood Cliffs: Prentice-Hall, 1968.

[23] R. F. Harrington, Time-Harmonic Electromagnetic Fields. New York: McGraw-Hill, 1961.

[24] P. Henrici, Discrete Variable Methods in Ordinary Differential Equations. New York: Wiley, 1962.

[25] R. S. Varga, Matrix Iterative Analysis. Englewood Cliffs: Prentice-Hall, 1962.

[26] W. H. Hayt, Engineering Electromagnetics, second edition. New York: McGraw-Hill, 1967.

[27] R. B. Adler, L. J. Chu, and R. M. Fano, Electromagnetic Energy Transmission and Radiation. New York: Wiley, 1965.

[28] H. P. Westman (editor), Reference Data for Radio Engineers, fourth edition. International Telephone and Telegraph Company, New York, 1956, pp. 128-129.

VII. ACKNOWLEDGMENTS

The author wishes to express his gratitude to Dr. David T. Stephenson, who guided this work, and to Dr. Robert E. Post for their assistance. Thanks are also given to the many others whose helpful comments aided this work. The excellent typing of the manuscript was done by Marcy Houck.

This work is dedicated to my wife Susan and my daughter Jill.

VIII. APPENDIX: COMPUTER PROGRAM LISTING

This program calculates the current distribution, input impedance, radiation resistance, efficiency, and directive gain for a NMHD. The NMHD is assumed to be a right-handed helix with a copper wire conductor. The excitation is assumed to be a slice voltage generator of one volt peak amplitude located at the midpoint of the antenna. The program consists of a main program and six subroutines, which are listed after the main program.

As written, the program allows a maximum of two hundred fifty-one segments to be used in the helix approximation. More segments can be used by changing the dimensioning statements. When compiled in H-level FORTRAN, the execution time for this program, using two hundred fifty-one segments to approximate the helix, is about fifty seconds on the IBM 360/65 computer.

While the program was written for copper conductors, other conductors can be used by changing line ninety-four in the main program.

Note that while the program is written to calculate directive gain, power gain can be calculated if desired. In order to calculate power gain, line one hundred forty-seven of the main program should be changed to read

```
CALL GAIND(RO,DTHET,PHI,PIN)
```

If power gain is calculated, line thirty of the main program should be changed to note this fact.

```
C       MAIN PROGRAM
C
C       THIS PROGRAM AND ITS ASSOCIATED SUBROUTINES CALCULATE THE CURRENT
C       DISTRIBUTION, INPUT IMPEDANCE, RADIATION RESISTANCE, EFFICIENCY,
C       AND DIRECTIVE GAIN FOR A HELICAL DIPOLE ANTENNA WITH
C       WAVE = FREE SPACE WAVELENGTH IN METERS.
C       THE CURRENT DISTRIBUTION IS CALCULATED FOR AN EXCITATION VOLTAGE
C       OF ONE VOLT PEAK LOCATED AT THE MIDPOINT OF THE ANTENNA.
C       THE ANTENNA IS ASSUMED TO BE A RIGHT-HANDED HELIX, THAT IS, THE
C       WIRE CONDUCTOR TRACES OUT THE PATH OF A RIGHT-HANDED SCREW.
C       NOTE THAT THE WIRE IS ASSUMED TO BE COPPER.
C
  1     FORMAT('1',' THE DIMENSIONS OF THE ANTENNA FOLLOW',/)
  2     FORMAT('0',' THE RADIUS OF THE WIRE IS',1PE16.6,'  METERS')
  3     FORMAT('0',' THE MEAN HELIX RADIUS IS ',1PE16.6,'  METERS')
  4     FORMAT('0',' THE HELIX HALFLENGTH IS  ',1PE16.6,'  METERS')
  5     FORMAT('0',' THE PITCH OF THE HELIX IS',1PE16.6,'  METERS')
  6     FORMAT('0',' THE HELIX PITCH ANGLE IS ',1PE16.6,'  DEGREES')
  7     FORMAT('0',' THE CURRENT IS NONZERO ALONG',T36,I3,T46,'SEGMENTS')
  8     FORMAT('0',' THE FREE SPACE WAVELENGTH IS',1PE13.6,'  METERS')
  9     FORMAT('1',' THE ELEMENTS OF Z ARE')
 10     FORMAT(T3,'I',T16,'Z(I)',T42,'I',T55,'Z(I)',T82,'I',T95,'Z(I)')
 11     FORMAT('1',' THE CURRENT DISTRIBUTION IS',T74,'THE EXCITATION CHEC
       1K IS')
 12     FORMAT('  I',T19,'C(I)',T37,'MAGNITUDE',T53,'PHASE',T82,'VCK(I)')
 13     FORMAT('0',' THE INPUT IMPEDANCE IS ',1P2E14.5,'  OHMS')
 14     FORMAT('0',' THE INPUT ADMITTANCE IS',1P2E14.5,'  MHOS')
 15     FORMAT('0',' THE AC RESISTANCE PER SEGMENT IS ',1PE14.5,'  OHMS')
 16     FORMAT(T7,'THETA',T21,'GTHETA',T36,'GPHI')
 17     FORMAT('1',' THE DIRECTIVE GAIN IS')
 20     FORMAT('1')
 21     FORMAT(E13.7)
 22     FORMAT(I3)
 23     FORMAT(I4,1P2E12.4,T40,I4,2E12.4,T80,I4,2E12.4)
 24     FORMAT(I4,1P4E14.5,T70,2E14.5)
```

```
 27    FORMAT(1P3E14.5)                                                 MAIN 036
 31    FORMAT('0',' THE INPUT POWER IS',T28,1PE14.5,'  WATTS')          MAIN 037
 32    FORMAT('0',' THE DISSIPATED POWER IS',T28,1PE14.5,'  WATTS')     MAIN 038
 33    FORMAT('0',' THE RADIATED POWER IS',T28,1PE14.5,'  WATTS')       MAIN 039
 34    FORMAT('0',' THE INPUT RESISTANCE IS',T35,1PE14.5,'  OHMS')      MAIN 040
 35    FORMAT('0',' THE DISSIPATION RESISTANCE IS',T35,1PE14.5,'  OHMS') MAIN 041
 36    FORMAT('0',' THE RADIATION RESISTANCE IS',T35,1PE14.5,'  OHMS')  MAIN 042
 37    FORMAT('0',' THE ANTENNA EFFICIENCY IS  ',F6.2,'  PERCENT')      MAIN 043
       COMPLEX Z(251),ZR(126,126),C(126),VCK(126),CI,ZIN,YIN            MAIN 044
       COMPLEX ZINP,YINP                                                MAIN 045
       DIMENSION R(3,251),B(3,251),THETD(91),GTHETA(91),GPHI(91)        MAIN 046
       COMMON /COA/ Z /COB/ ZR /COC/ C /COD/ VCK                        MAIN 047
       COMMON /CONST/ CI,PI,XMU,EPSLN,BA,BH,HAFLEN,PITCH,PANG,NS,NEP,   MAIN 048
      1WAVE,OMEG,BETA,DZ,TLEN                                           MAIN 049
       EQUIVALENCE (ZR(1,1),R(1,1)),(ZR(1,4),B(1,1))                    MAIN 050
       EQUIVALENCE (ZR(1,7),GTHETA(1)),(ZR(1,8),GPHI(1))                MAIN 051
       EQUIVALENCE (ZR(1,9),THETD(1))                                   MAIN 052
       PI = 3.14159265                                                  MAIN 053
C      XMU = THE PERMEABILITY OF FREE SPACE                             MAIN 054
       XMU = 4.0E-7*PI                                                  MAIN 055
C      EPSLN = THE PERMITTIVITY OF FREE SPACE                           MAIN 056
       EPSLN = 8.854E-12                                                MAIN 057
       CI = (0.,1.)                                                     MAIN 058
C      BA = THE RADIUS OF THE WIRE IN METERS                            MAIN 059
 50    READ(5,21, END=51) BA                                            MAIN 060
       WRITE(6,1)                                                       MAIN 061
       WRITE(6,2) BA                                                    MAIN 062
C      BH = THE MEAN HELIX RADIUS IN METERS                             MAIN 063
       READ(5,21) BH                                                    MAIN 064
       WRITE(6,3) BH                                                    MAIN 065
C      HAFLEN = THE HELIX HALF LENGTH IN METERS                         MAIN 066
       READ(5,21) HAFLEN                                                MAIN 067
       WRITE(6,4) HAFLEN                                                MAIN 068
C      PITCH = THE PITCH OF THE HELIX                                   MAIN 069
       READ(5,21) PITCH                                                 MAIN 070
```

```
      WRITE(6,5) PITCH
C     PANG = HELIX PITCH ANGLE IN RADIANS
      PANG = ATAN2(PITCH,(PI*2.*BH))
C     PANGL = HELIX PITCH ANGLE IN DEGREES
      PANGL = 180.*PANG/PI
      WRITE(6,6) PANGL
C     NS = NUMBER OF SEGMENTS WITH NON-ZERO CURRENT
      READ(5,22) NS
      WRITE(6,7) NS
C     WAVE = THE FREE SPACE WAVELENGTH IN METERS
      READ(5,21) WAVE
      WRITE(6,8) WAVE
C     DZ = Z-DISTANCE BETWEEN ADJACENT SEGMENTS IN METERS
      DZ = 2.*HAFLEN/(NS+1)
C     TLEN = THE LENGTH OF EACH SEGMENT IN METERS
      TLEN = DZ*SQRT((2.*BH*PI/PITCH)**2+1)
C     NEP = THE ORDER OF THE REDUCED IMPEDANCE MATRIX ZR
      NEP = (NS+1)/2
C     OMEG = THE ANGULAR FREQUENCY IN RADIAN PER SECOND
      OMEG = 2.99793E8/WAVE*2.*PI
C     BETA = THE PHASE CONSTANT OF FREE SPACE IN RADIANS PER METER
      BETA = 2.*PI/WAVE
C     RSQ = AC RESISTANCE PER SQUARE FOR COPPER
      RSQ = 2.61E-7*SQRT(3.E+8/WAVE)
C     SQUARS = NUMBER OF SQUARES PER SEGMENT
      SQUARS = TLEN/(2.*PI*BA)
C     RSEG = AC RESISTANCE PER SEGMENT
      RSEG = RSQ*SQUARS
      WRITE(6,15) RSEG
      CALL CAZZ
C     MODIFY Z TO ACCOUNT FOR THE FINITE CONDUCTIVITY OF COPPER
      Z(1)=Z(1)+RSEG
      WRITE(6,9)
      WRITE(6,10)
      ILIN=NS+2.5
```

```
      WRITE(6,23) (I,Z(I),I=1,ILIN)
      CALL CAZR(NS)
C     INITIALIZE C TO THE EXCITATION VOLTAGE
      NEPM1=NEP-1
      DO 201 I=1,NEPM1
  201 C(I)=(0.,0.)
      C(NEP)=(1.,0.)
      CALL SGEA(NEP)
      WRITE(6,11)
      WRITE(6,12)
      CALL CAZR(NS)
      CALL VCHK(NEP)
      PSUM=0.
      DO 103 I=1,NEP
      CMAG2=REAL(C(I))**2+AIMAG(C(I))**2
      CMAG=SQRT(CMAG2)
      PSUM=PSUM+CMAG2
      CPHA=ATAN2(AIMAG(C(I)),REAL(C(I)))*180./PI
  103 WRITE(6,24) I,C(I),CMAG,CPHA,VCK(I)
      YINP=C(NEP)
      ZINP=1./YINP
      WRITE(6,13) ZINP
      WRITE(6,14) YINP
      PIN=REAL(C(NEP))/2.
      PDISS = RSEG*(PSUM-CMAG2/2.)
      PRAD=PIN-PDISS
      RIN=REAL(ZINP)
      RDISS=PDISS*RIN/PIN
      RRAD=PRAD*RIN/PIN
      EFFIC=PRAD/PIN*100.
      WRITE(6,31) PIN
      WRITE(5,32) PDISS
      WRITE(6,33) PRAD
      WRITE(6,34) RIN
      WRITE(6,35) RDISS
```

```
      WRITE(6,36) RRAD
      WRITE(6,37) EFFIC
      RO=1.E+4
      DTHET=2.
      PHI=0.
      CALL CORD
      CALL GAIND(RO,DTHET,PHI,PRAD)
      WRITE(6,17)
      WRITE(6,16)
      IMAX=90/DTHET+1.5
      WRITE(6,27) (THETD(I),GTHETA(I),GPHI(I),I=1,IMAX)
      WRITE(6,20)
      GO TO 50
   51 CONTINUE
      STOP
      END
```

```
      SUBROUTINE CAZZ
C
C     THIS SUBROUTINE IS USED TO CALCULATE THE ELEMENTS OF Z
C
      COMPLEX Z(251),PSIA,PSIB,PSIC,CI,RT,CMPLX
      COMMON /COA/ Z
      COMMON /CONST/ CI,PI,XMU,EPSLN,BA,BH,HAFLEN,PITCH,PANG,NS,NEP,
     1WAVE,OMEG,BETA,DZ,TLEN
      D2=BH*COS(PANG)
      SPANG=SIN(PANG)
      P2=2.*PI/PITCH
      D3=2.*BH**2
      PSIB=(0.0,0.0)
      PSIC=(0.0,0.0)
      NSP1=NS+1
      NSP2=NS+2
      AL=DZ/2.*SQRT((2.*BH*PI/PITCH)**2+1)
      B1=OMEG*XMU*4.*AL**2
      CPANG2=COS(PANG)**2
      SPANG2=SPANG**2
      AI2=2.*AL
      TO3AL3=2.*AL**3/3.
      BET3O6=BETA**3/6.
      RPIAL8=1./(PI*AL*8.)
      XKD=BETA*AL
      XKD2=XKD**2
      XKD3=XKD*XKD2
      XKD4=XKD2**2
      ROMEP=1./(OMEG*EPSLN)
C     EVALUATE THE ELEMENTS OF Z
      DO 210 I=1,NSP1
      ZK=DZ*(I-1)
      ZETA=D2*SIN(P2*ZK)+ZK*SPANG
      RADI2=D3*(1.-COS(P2*ZK))+ZK**2
      RADI=SQRT(RADI2)
```

```
      RHO=SQRT(RADI2-ZETA**2)                                          CAZZ 036
      PSIA=PSIB                                                        CAZZ 037
      PSIB=PSIC                                                        CAZZ 038
      IF(RHO-AL)211,211,212                                            CAZZ 039
  211 RHO=AL                                                           CAZZ 040
  212 IF(RADI-10.*AL)213,213,214                                       CAZZ 041
  213 RT=COS(-BETA*RADI)+CI*SIN(-BETA*RADI)                            CAZZ 042
      ZA=ZETA+AL                                                       CAZZ 043
      ZAM=ZETA-AL                                                      CAZZ 044
      SZA=SQRT(RHO**2+ZA**2)                                           CAZZ 045
      SZAM=SQRT(RHO**2+ZAM**2)                                         CAZZ 046
      AI1=ALOG((ZA+SZA)/(ZAM+SZAM))                                    CAZZ 047
      AI3=(ZA*SZA-ZAM*SZAM+RHO**2*AI1)/2.                              CAZZ 048
      AI4=AI2*(RHO**2+ZETA**2)+TO3AL3                                  CAZZ 049
      PSI1=AI1-BETA**2/2.*(AI3-2.*RADI*AI2+RADI**2*AI1)                CAZZ 050
     0PSI2=-BETA*(AI2-RADI*AI1)+BET3O6*(AI4-3.*RADI*AI3                CAZZ 051
     1+3.*RADI**2*AI2-RADI**3*AI1)                                     CAZZ 052
      PSIC=RT*RPIAL8*CMPLX(PSI1,PSI2)                                  CAZZ 053
      GO TO 215                                                        CAZZ 054
  214 RT=COS(-BETA*RADI)+CI*SIN(-BETA*RADI)                            CAZZ 055
      ZRA=ZETA/RADI                                                    CAZZ 056
      DR=AL/RADI                                                       CAZZ 057
      ZR2=ZRA**2                                                       CAZZ 058
      ZR4=ZR2**2                                                       CAZZ 059
      DR2=DR**2                                                        CAZZ 060
      H=(-1.0+3.0*ZR2)/6.0                                             CAZZ 061
      H1=(3.0-30.0*ZR2+35.0*ZR4)/40.0                                  CAZZ 062
      A0=1.0+H*DR2+H1*DR2**2                                           CAZZ 063
      A1=H*DR+H1*DR2*DR                                                CAZZ 064
      A2=-ZR2/6.0-DR2/40.0*(1.0-12.0*ZR2+15.0*ZR4)                     CAZZ 065
      A3=DR/60.0*(3.0*ZR2-5.0*ZR4)                                     CAZZ 066
      A4=ZR4/120.0                                                     CAZZ 067
      PSI1=A0+XKD2*A2+XKD4*A4                                          CAZZ 068
      PSI2=XKD*A1+XKD3*A3                                              CAZZ 069
      PSIC=RT/(4.*PI*RADI)*CMPLX(PSI1,PSI2)                            CAZZ 070
```

```
215  IF(I-2) 218,216,217                                         CAZZ 071
216  PSIA=PSIC                                                   CAZZ 072
217 OZ(I-1)=CI*(B1*(CPANG2*COS(P2*DZ*(I-2))+SPANG2)*PSIB          CAZZ 073
   1+(PSIA-2.*PSIB+PSIC)*ROMEP)                                  CAZZ 074
218  CONTINUE                                                    CAZZ 075
210  CONTINUE                                                    CAZZ 076
     RETURN                                                      CAZZ 077
     END                                                         CAZZ 078
```

```
      SUBROUTINE CAZR(NS)
C
C     THIS SUBROUTINE IS USED TO CALCULATE THE ELEMENTS OF ZR
C
      COMPLEX Z(251),ZR(126,126)
      COMMON /COA/ Z /COB/ ZR
      NEP=(NS+1)/2
      NEPM=NEP-1
      NSP2=NS+2
      DO 220 I=1,NEP
      DO 220 J=1,NEP
  220 ZR(I,J)=Z(IABS(I-J)+1)
      DO 221 I=1,NEPM
  221 ZR(NEP,I)=2.0*ZR(NEP,I)
      DO 222 I=1,NEPM
      DO 222 J=1,NEPM
  222 ZR(I,J)=ZR(I,J)+Z(NSP2-I-J)
      RETURN
      END
```

```
      SUBROUTINE SGEA(N)
C
C     THIS SUBROUTINE SOLVES THE COMPLEX LINEAR SYSTEM A*X=B WHERE
C     A = N BY N COMPLEX COEFFICIENT MATRIX (DESTROYED)
C     N = NUMBER OF EQUATIONS AND UNKNOWNS
C     B = N ELEMENT VECTOR (REPLACED BY SOLUTION VECTOR X)
C     X = N ELEMENT UNKNOWN VECTOR (SOLUTION)
C     THE METHOD USED IS GAUSS ELIMINATION WITH PARTIAL PIVOTING.
C     THE PIVOT ELEMENT IS THAT ELEMENT IN THE PIVOT COLUMN WITH
C     GREATEST NORM WHERE THE NORM USED IS
C     NORM(A) = |RE(A)| + |IM(A)|
C     THE EVALUATION OF THIS NORM IS MUCH FASTER THAN FOR THE EUCLIDEAN
C     NORM AND GIVES NEARLY AS GOOD RESULTS.
C
      COMPLEX A(126,126),B(126),RPIV,SAVE
      COMMON /COB/ A /COC/ B
      NP1=N+1
      NM1=N-1
C     FORWARD SOLUTION
      DO 50 J=1,NM1
      J1=J+1
      PNORM=0.
      IMAX=J
C     SEARCH JTH COLUMN FOR PIVOT
      DO 11 I=J,N
      ANORM=ABS(REAL(A(I,J)))+ABS(AIMAG(A(I,J)))
      IF(PNORM-ANORM) 10,11,11
   10 PNORM=ANORM
      IMAX=I
   11 CONTINUE
C     INTERCHANGE ROWS IF NECESSARY
      IF(IMAX-J) 20,22,20
   20 DO 21 I=J,N
      SAVE=A(J,I)
      A(J,I)=A(IMAX,I)
```

```
 21     A(IMAX,I)=SAVE                                            SGEA 036
        SAVE=B(J)                                                 SGEA 037
        B(J)=B(IMAX)                                              SGEA 038
        B(IMAX)=SAVE                                              SGEA 039
C       DIVIDE PIVOT EQUATION BY PIVOT                            SGEA 040
 22     RPIV=(1.E+00,0.E+00)/A(J,J)                               SGEA 041
        DO 30 I=J,N                                               SGEA 042
 30     A(J,I)=A(J,I)*RPIV                                        SGEA 043
        B(J)=B(J)*RPIV                                            SGEA 044
C       ELIMINATE ELEMENTS BELOW DIAGONAL IN JTH COLUMN           SGEA 045
        DO 50 I=J1,N                                              SGEA 046
        SAVE=A(I,J)                                               SGEA 047
        DO 40 JJ=J,N                                              SGEA 048
 40     A(I,JJ)=A(I,JJ)-SAVE*A(J,JJ)                              SGEA 049
        B(I)=B(I)-SAVE*B(J)                                       SGEA 050
 50     CONTINUE                                                  SGEA 051
        B(N)=B(N)/A(N,N)                                          SGEA 052
C       BACK SUBSTITUTION                                         SGEA 053
        DO 60 I=1,NM1                                             SGEA 054
        IR=N-I                                                    SGEA 055
        DO 60 J=1,I                                               SGEA 056
        JC=NP1-J                                                  SGEA 057
 60     B(IR)=B(IR)-A(IR,JC)*B(JC)                                SGEA 058
        RETURN                                                    SGEA 059
        END                                                       SGEA 060
```

```
      SUBROUTINE VCHK(N)
C
C     THIS SUBROUTINE IS USED TO MULTIPLY THE CURRENT DISTRIBUTION C BY
C     THE REDUCED IMPEDANCE ZR TO FORM THE VOLTAGE CHECK MATRIX VCK.
C
      COMPLEX ZR(126,126),C(126),VCK(126)
      COMMON /COB/ ZR /COC/ C /COD/ VCK
      DO 100 I=1,N
      VCK(I)=(0.0,0.0)
      DO 100 J=1,N
  100 VCK(I)=VCK(I)+ZR(I,J)*C(J)
      RETURN
      END
```

```
      SUBROUTINE CORD
C
C     THIS SUBROUTINE IS USED TO GENERATE THE FOLLOWING ELEMENTS
C     R(1,I) = X COORDINATE OF MIDPOINT OF ITH SEGMENT IN METERS
C     R(2,I) = Y COORDINATE OF MIDPOINT OF ITH SEGMENT IN METERS
C     R(3,I) = Z COORDINATE OF MIDPOINT OF ITH SEGMENT IN METERS
C     B(1,I) = X COMPONENT OF UNIT VECTOR ALONG ITH SEGMENT
C     B(2,I) = Y COMPONENT OF UNIT VECTOR ALONG ITH SEGMENT
C     B(3,I) = Z COMPONENT OF UNIT VECTOR ALONG ITH SEGMENT
C
      COMPLEX ZR(126,126),CI
      DIMENSION R(3,251),B(3,251)
      COMMON /COB/ ZR
      COMMON /CONST/ CI,PI,XMU,EPSLN,BA,BH,HAFLEN,PITCH,PANG,NS,NEP,
     1WAVE,OMEG,BETA,DZ,TLEN
      EQUIVALENCE (ZR(1,1),R(1,1)),(ZR(1,4),B(1,1))
      P2=2.*PI/PITCH
      SP=SIN(PANG)
      CP=COS(PANG)
      DO 10 I=1,NEP
      Z=DZ*(I-NEP)
      P2Z=P2*Z
      SP2Z=SIN(P2Z)
      CP2Z=COS(P2Z)
      R(1,I)=-BH*SP2Z
      R(2,I)= BH*CP2Z
      R(3,I)= Z
      B(1,I)=-CP*CP2Z
      B(2,I)=-CP*SP2Z
   10 B(3,I)= SP
      NM=NEP-1
      DO 11 I=1,NM
      K=NS+1-I
      R(1,K)=-R(1,I)
      R(2,K)= R(2,I)
```

```
      R(3,K)=-R(3,I)                                                    CORD 036
      B(1,K)= B(1,I)                                                    CORD 037
      B(2,K)=-B(2,I)                                                    CORD 038
   11 B(3,K)= B(3,I)                                                    CORD 039
      RETURN                                                            CORD 040
      END                                                               CORD 041
```

```
      SUBROUTINE GAIND(RO,DTHET,PHI,PRAD)
C
C     THIS SUBROUTINE IS USED TO CALCULATE THE DIRECTIVE GAIN FOR BOTH
C     POLARIZATIONS AT A FIELD POINT WITH SPHERICAL COORDINATES
C     RO, THETA, PHI WHERE
C     RO = RADIUS IN METERS
C     THETA = POLAR ANGLE IN DEGREES
C     PHI = AZIMUTHAL ANGLE IN DEGREES
C     THE GAIN IS EVALUATED FOR THETA RANGING FROM 0 TO 90 DEGREES IN
C     STEPS OF DTHET DEGREES ALONG A PATH WITH CONSTANT RO AND PHI
C     XF = X COORDINATE OF FIELD POINT IN METERS
C     YF = Y COORDINATE OF FIELD POINT IN METERS
C     ZF = Z COORDINATE OF FIELD POINT IN METERS
C     ETHETA = THETA COMPONENT OF FAR FIELD
C     EPHI = PHI COMPONENT OF FAR FIELD
C     GTHETA(J) = GAIN OF THETA POLARIZATION FOR THETA=J*ITHET
C     GPHI(J) = GAIN OF PHI POLARIZATION FOR THETA=J*ITHET
C     PRAD = RADIATED POWER
C
      COMPLEX ZR(126,126),C(126),CI,C1,C2,ETHETA,EPHI
      DIMENSION R(3,251),B(3,251),THETD(91),GTHETA(91),GPHI(91)
      COMMON /COB/ ZR /COC/ C
      COMMON /CONST/ CI,PI,XMU,EPSLN,BA,BH,HAFLEN,PITCH,PANG,NS,NEP,
     1WAVE,OMEG,BETA,DZ,TLEN
      EQUIVALENCE (ZR(1,1),R(1,1)),(ZR(1,4),B(1,1))
      EQUIVALENCE (ZR(1,7),GTHETA(1)),(ZR(1,8),GPHI(1))
      EQUIVALENCE (ZR(1,9),THETD(1))
      PHIR=PHI*PI/180.
      SPH=SIN(PHIR)
      CPH=COS(PHIR)
      ROSPH=RO*SPH
      ROCPH=RO*CPH
      ROK=BETA*RO
      T1=-OMEG*XMU*TLEN/(4.*PI*RO)
      C1=T1*(CI*COS(ROK)+SIN(ROK))
```

```
      RKRO=BETA/RO
      PISO=PRAD/(4.*PI*RO**2)
      THETR=0.
      DTHR=DTHET*PI/180.
      IMAX=90/DTHET+1.5
      DO 30 I=1,IMAX
      STH=SIN(THETR)
      CTH=COS(THETR)
      XF=ROCPH*STH
      YF=ROSPH*STH
      ZF=RO*CTH
      ETHETA=(0.,0.)
      EPHI=(0.,0.)
      DO 20 J=1,NS
      BTH=(B(1,J)*CPH+B(2,J)*SPH)*CTH-B(3,J)*STH
      BPH=-B(1,J)*SPH+B(2,J)*CPH
      RDR=R(1,J)*XF+R(2,J)*YF+R(3,J)*ZF
      ANG=RKRO*RDR
      IF(J-NEP) 17,17,18
   17 C2=C(J)
      GO TO 19
   18 C2=C(NS+1-J)
   19 C2=C2*(COS(ANG)+CI*SIN(ANG))
      ETHETA=ETHETA+BTH*C2
   20 EPHI=EPHI+BPH*C2
      ETHETA=C1*ETHETA
      EPHI=C1*EPHI
      PTH=(REAL(ETHETA)**2+AIMAG(ETHETA)**2)/754.
      PPH=(REAL(EPHI)**2+AIMAG(EPHI)**2)/754.
      THETD(I)=(I-1)*DTHET
      GTHETA(I)=PTH/PISO
      GPHI(I)=PPH/PISO
   30 THETR=THETR+DTHR
      RETURN
      END
```